Synthesis and Characterization of Novel Functionalized Polysiloxanes and Their Application in Model and Catalytic Reactions, and in Chromatography

❖ ❖ ❖

Synthese und Charakterisierung neuer funktionalisierter Polysiloxane und ihre Anwendung in Modell- und katalytischen Reaktionen und in der Chromatographie

Dissertation

der Fakultät für Chemie und Pharmazie

der Eberhard-Karls-Universität Tübingen

zur Erlangung des Grades eines Doktors

der Naturwissenschaften

2002

vorgelegt von

Thomas Salesch

Tag der mündlichen Prüfung: 18.01.2002

Dekan: Prof. Dr. H. Probst

1. Berichterstatter: Prof. Dr. E. Lindner

2. Berichterstatter: Prof. Dr. H. A. Mayer

Meiner Frau Gudrun

Die vorliegende Arbeit wurde am

Institut für Anorganische Chemie der

Eberhard-Karls-Universität Tübingen

unter Leitung von Prof. Dr. rer. nat. Ekkehard Lindner

angefertigt.

Meinem Doktorvater

Herrn Prof. Dr. Ekkehard Lindner,

danke ich herzlich für die interessante Themenstellung,

die Bereitstellung ausgezeichneter Arbeitsbedingungen,

für wertvolle Anregungen und Diskussionen

sowie sein stetes Interesse an dieser Arbeit.

CONTENTS

Contents

1. INTRODUCTION

The anchoring of reactive centers, in particular catalytically active transition metal complexes, to an inert support is a field of increasing interest in terms of academic as well as commercial research [1–14]. Such materials are able to combine the advantages of homogenous and heterogeneous catalysis: the catalyst becomes easily separable from the reaction products and it can be reused in several runs without an essential loss of activity. On the other hand, the reactive centers are well defined and the improvement of their properties is not only empirical. Due to the homogenous character of the catalytic reaction the activities and selectivities are high [15].

However, there are still specific problems with such systems which inhibited the commercial breakthrough of these types of catalysts. They can leach from the support during the catalytic reaction. Furthermore the heterogenization of complexes leads to reduced mobility of the reactive centers causing lower activities and selectivities of the anchored catalysts compared to their homogenous counterparts [16].

A versatile approach to reduce or even eliminate these problems is the introduction of the concept of interphase [17–21]. In the presence of a stationary phase (e. g. an anchored metal complex) and a mobile phase (solvent, gaseous or liquid reactant) a penetration of both phases on a molecular level takes place (Figure 1). This state is designated as 'interphase' since no homogenous phase is formed. However, interphases are able to imitate homogenous conditions providing favorable activities in different types of catalytic reactions without any essential metal leaching. A typical approach for the generation of stationary phases in interphase chemistry is the sol-gel process, which offers a convenient route for the preparation of suitable polysiloxane networks under smooth and low temperature conditions.

Simultaneous co-condensation of T-silyl functionalized metal complexes or ligands with various alkoxysilanes or organosilanes provides materials, in which the reactive centers are nearly homogeneously distributed across a chemical and thermal inert carrier matrix [21–28]. Since the polysiloxane-bound active centers are readily accessible even for larger molecules, those kinds of inorganic-organic hybrid materials are predestinated for catalytic reactions [29–33].

A separate introduction for the application of interphase systems in chromatography is given in part 2.4.1..
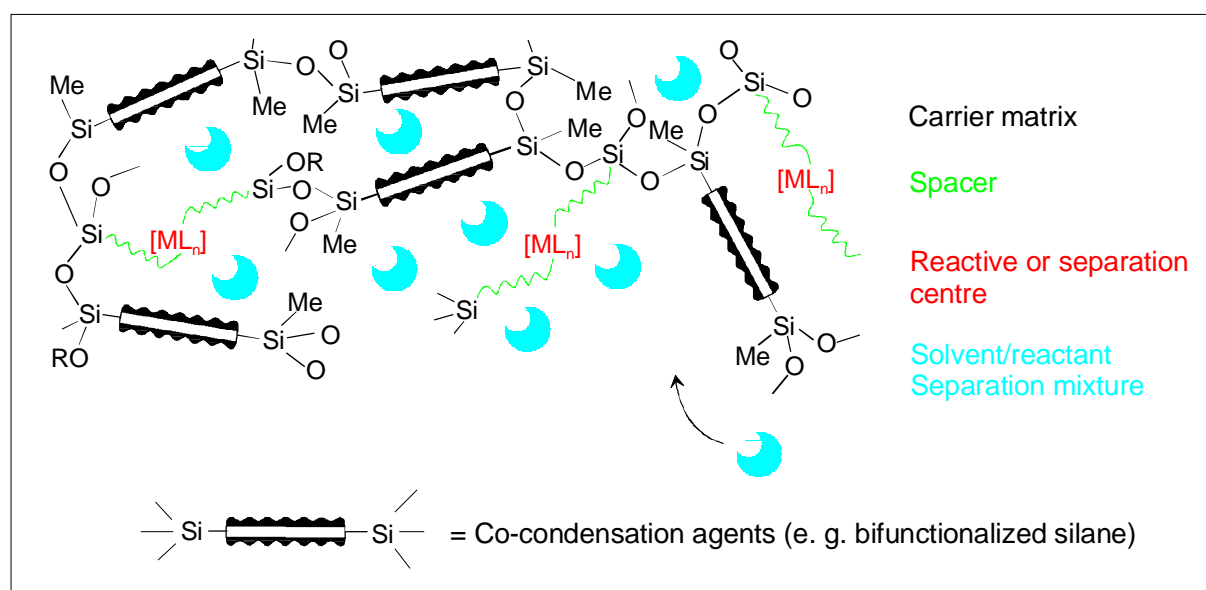
Figure 1. Schematic description of an interphase.

2. GENERAL SECTION

2. 1. Hydroformylation of 1-Hexene in Interphases – the Influence of Different Kinds of Inorganic-Organic Hybrid Co-Condensation Agents on the Catalytic Activity

2.1.1. Introduction

In this chapter of the thesis a novel mono-T-silyl functionalized triphenylphosphine ligand was prepared by a simple coupling reaction of (*p*-aminophenyl)diphenylphosphine and 3-triethoxysilylpropylisocyanate. The corresponding carbonylchlorobisphosphinerhodium(I) complex ClRh(CO)[PPh$_2$C$_6$H$_4$NHCONH(CH$_2$)$_3$Si(OEt)$_3$]$_2$ was synthesized in order to be sol-gel processed with various amounts of different D-silyl and T-silyl bifunctionalized co-condensation agents. The polysiloxane matrices and the active rhodium centers were investigated by means of multinuclear solid state NMR (^{13}C, ^{29}Si, ^{31}P) and dynamic NMR measurements. The rhodium containing xerogels were applied in the hydroformylation of 1–hexene. These stationary phases show remarkable catalytic activities independent on the solvent. An enhancement of the activities is achieved when T-silyl bifunctionalized co-condensation agents are used to build up the carrier matrix.

2.1.2. Synthesis of the T-Silyl Functionalized Ligand 2(T⁰) and of the Monomeric Rhodium(I) Complex 3(T⁰)

The triphenylphosphine analogous ligand **2(T^0)** was obtained in good yields as a waxy colorless solid by the reaction of (*p*-aminophenyl)diphenylphosphine (**1**) with one equivalent of triethoxysilylpropylisocyanate in dichloromethane. The modified Vaska complex **3(T^0)** can be easily prepared by the reaction of **2(T^0)** with a half equivalent of [μ-ClRh(CO)$_2$]$_2$ in benzene (Scheme 1). Both compounds were characterized by ^{1}H, ^{13}C{^{1}H}, ^{31}P{^{1}H} NMR,

Scheme 1.
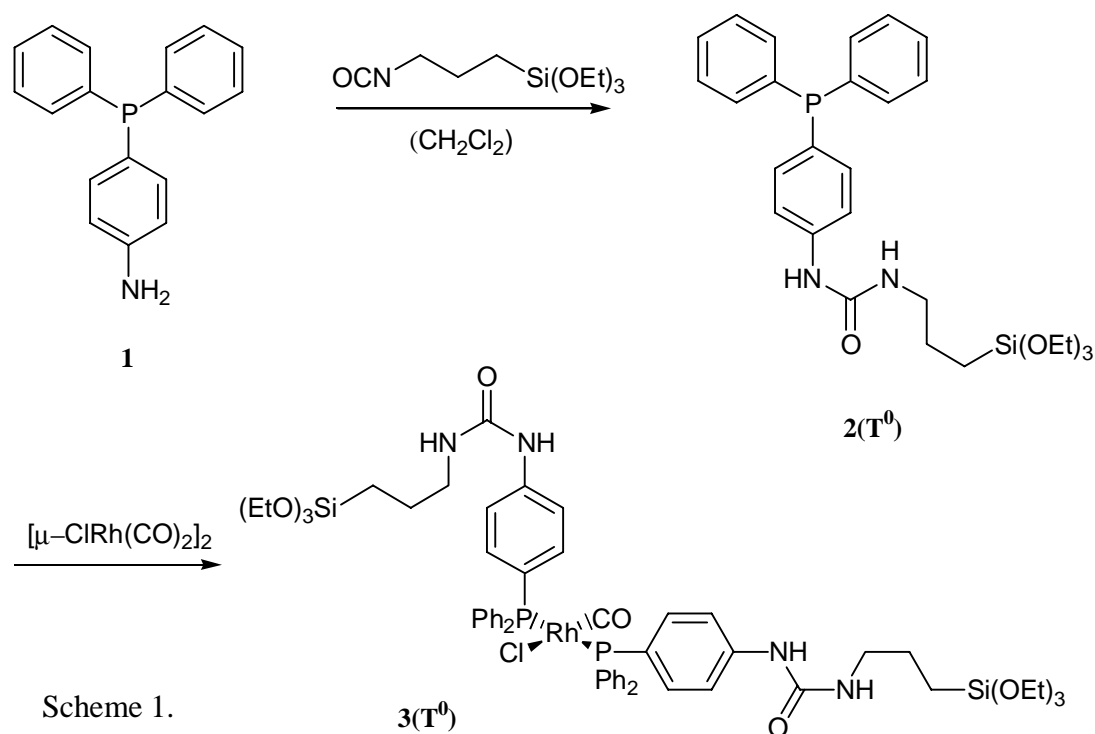
and IR spectroscopy, as well as mass spectrometry, and elemental analysis. In the ^{31}P{^{1}H} and ^{29}Si{^{1}H} NMR spectra of **2(T^0)** each one signal is observed at $\delta = -5.5$ and -45.1, respectively. Compared to triphenylphosphine the *para*-positioned spacer function exerts nearly no influence on the chemical shift of the ^{31}P nucleus in **2(T^0)**. The composition of the rhodium complex **3(T^0)** was corroborated by its EI mass spectrum showing the molecular peak at $m/z = 1214$. Only one doublet with a $^1J_{RhP}$ coupling constant of 124.7 Hz occurs in the

$^{31}P\{^{1}H\}$ NMR spectrum of complex $\mathbf{3(T^0)}$, which is indicative of a *trans*-position of the phosphine ligands. A characteristic absorption at 1980 cm^{-1} in the IR spectrum of $\mathbf{3(T^0)}$ is assigned to the carbonyl stretching vibration. Other analytic data are summarized in the experimental part.

2.1.3. Sol-Gel Processing of $\mathbf{2(T^0)}$ and $\mathbf{3(T^0)}$

The xerogels **X2a** and **X2b** were prepared by sol-gel processing of the monomeric T-silyl functionalized ligand $\mathbf{2(T^0)}$ with the co-condensation agent $\mathbf{4(D^0)}$ and $\mathbf{5(D^0)}$, respectively. In the case of **X3a–d** the rhodium complex $\mathbf{3(T^0)}$ was condensed into a matrix consisting of the co-condensation agents $\mathbf{4(D^0)}$, $\mathbf{4(T^0)}$, $\mathbf{5(D^0)}$, and $\mathbf{5(T^0)}$ (Table 1, Scheme 2).

$$4(\mathbf{D^0}) \qquad 4(\mathbf{T^0})$$

$$5(\mathbf{D^0}) \qquad 5(\mathbf{T^0})$$
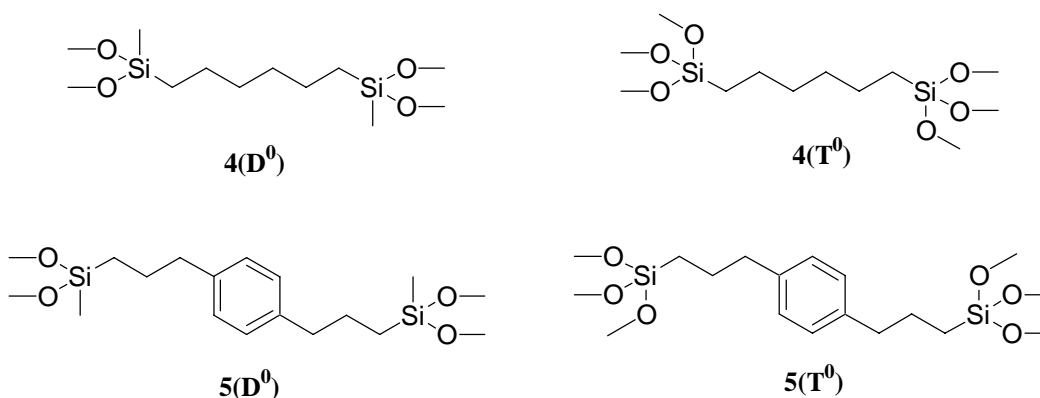
T = T type of silicon atom (three oxygen neighbours)
D = D type of silicon atom (two oxygen neighbours)

Scheme 2.

The properties of such materials strongly depend on the reaction conditions during the entire sol-gel process such as concentration of the monomers, type of solvent, temperature, and kind of catalyst. All sol-gel processes were carried out in THF with an excess of water and tetrabutylammoniumfluoride as catalyst. To guarantee reproducible materials uniform reaction conditions were maintained.

Table 1

Labeling of the compounds

Precursor	Co-condensation agent	Ideal T/D or T/T ratio	Xerogel
$2(T^0)$	$4(D^0)$	1 : 5	X2a
$2(T^0)$	$5(D^0)$	1 : 5	X2b
$3(T^0)$	$4(D^0)$	1 : 20	X3a
$3(T^0)$	$5(D^0)$	1 : 20	X3b
$3(T^0)$	$4(T^0)$	1 : 20	X3c
$3(T^0)$	$5(T^0)$	1 : 20	X3d

2.1.4. Solid State NMR Spectroscopic Investigations

Due to the amorphous nature of these materials, solid state NMR spectroscopy plays an important role in investigating the structure and the dynamic behavior of xerogels [34-36]. ^{29}Si NMR spectroscopy enables the characterization of the carrier matrix and the degree of condensation. ^{13}C and ^{31}P CP/MAS NMR spectroscopy allows an insight into the hydrocarbon regions and the reactive center, respectively (Figure 2).

2.1.4.1. ^{29}Si CP/MAS NMR Spectroscopy and Mobility of the Matrix

As a result of an incomplete condensation the ^{29}Si CP/MAS NMR spectra of the above-mentioned xerogels reveal signals of various substructures with corresponding D^i- and T^n-functions. Typical chemical shifts are δ = –4.8 (D^0), –14.3 (D^1), –22.3 (D^2), –58.2 (T^2), and –67.7 (T^3). They remain unchanged with respect to the stoichiometric composition of the materials and the kind of co-condensate. All silicon atoms in the polysiloxane matrix are in
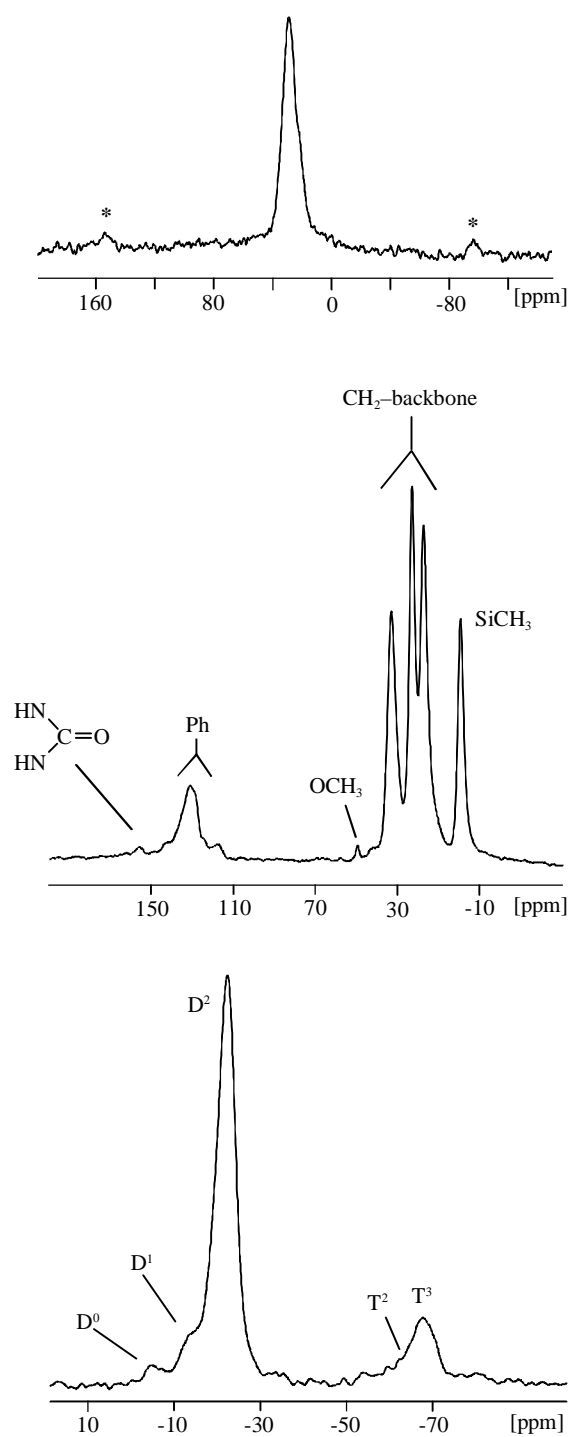
Figure 2. Solid state NMR spectra; top: [31]P CP/MAS of **X3d**; middle: [13]C CP/MAS of **X2a**; bottom: [29]Si CP/MAS of **X3a** (* rotational side bands).

Table 2

Relative I_0, T_{SiH}, and $T_{1\rho H}$ data of the silyl species in the xerogels

Xerogel	Relative I_0 data of D and T species[a]					Degree of condensation [%]		T_{SiH} [ms][c]					$T_{1\rho H}$ [ms][d]
	D⁰	D¹	D²	T²	T³	D	T	D⁰	D¹	D²	T²	T³	
X2a	1.5	17.4	100	6.1	20.8	92	93	F	f	1.24	f	1.43	7.1
X2b	2.0	16.1	100	2.6	18.7	92	96	F	f	1.45	f	1.83	6.8
X3a	e	100ᵇ	91.3ᵇ	1.3ᵇ	3.9ᵇ	74	95	E	1.02	1.28	f	1.11	6.3
X3b	e	55.2ᵇ	100ᵇ	1.6ᵇ	8.6ᵇ	82	95	E	0.96	1.22	f	1.15	5.8
X3c	e	e	e	31.6	100		91	E	e	e	1.15	2.02	6.0
X3d	e	e	e	42.2	100		90	E	e	e	0.67	1.52	5.1

[a] I_0 values calculated according to ref. [39]. [b] Determined via deconvolution of ^{29}Si CP/MAS NMR spectra (T_c = 5 ms).
[c] Determined by contact time variation. [d] Determined via ^{29}Si with the experiment according to ref. [39]. [e] Species not detectable.
[f] Intensity to low for a precise determination of T_{SiH}.

direct proximity of protons, thus silyl species are detectable via cross polarization [37,38]. Therefore the degree of condensation of D- and T-silyl functions were determined by contact time variation experiments (Table 2) [28,39]. However, due to the very low concentration of the T-groups in the xerogels **X3a** and **X3b** they can hardly be detected. Therefore the quantification of these silyl functions with contact time variation experiments is not feasible within a reasonable time and hence was carried out by deconvolution of the ^{29}Si CP/MAS spectra. In all above-mentioned xerogels the degrees of condensation range from 74 to 92 % and 90 to 96 % for the D- and T-groups, respectively. These results are in agreement with former investigations [40, 41].

2.1.4.2. ^{31}P CP/MAS NMR Spectroscopy and Mobility of the Reactive Center

In the ^{31}P CP/MAS NMR spectra of the polysiloxane-bound phosphines **X2a**, **b** one signal is observed at – 6.3 and – 6.7 ppm, respectively. Also only one broad signal with a chemical shift at about 29 ppm occurs in the ^{31}P CP/MAS NMR spectra of the rhodium containing polymers **X3a-d**. These results remind of the ligand and the monomeric rhodium(I) complex measured in solution. No other phosphine species is detectable in the freshly synthesized polymers, but exposure to air for some hours leads to the formation of phosphine oxide.

Due to higher values of the cross polarization constant T_{PH} (Table 3) the reactive centers (free phosphine ligand) in **X2a** and **X2b** show an enhanced mobility compared to the polysiloxane-bound rhodium complexes in **X3a-d**. Obviously the P-coordination of the ligands enables a fast magnetization transfer for all types of co-condensates. Furthermore it can be demonstrated, that the rhodium(I) centers in the T/D-materials **X3a**, **b** are slightly

more mobile than those in the T/T-polymers **X3c**, **d**. These results are in a good agreement

with former investigations [28,41].

Table 3

$T_{1\rho H}$ (via ^{31}P) and T_{PH} parameters of the xerogels

Xerogel	$T_{1\rho H}$ [ms][a]	T_{PH} [ms][b]
X2a	8.3	2.05
X2b	6.5	1.94
X3a	4.6	0.52
X3b	7.4	0.48
X3c	10.8	0.32
X3d	6.9	0.29

[a] Determined via ^{31}P according to ref. [39]. [b] Determined via contact time variation.

2.1.4.3. ^{13}C CP/MAS NMR Spectroscopy

The ^{13}C CP/MAS NMR spectra of **X2a**, **X3a**, and **X3c** reveal a broad group of signals

in the aromatic region, which stems from the phenyl carbon atoms of the functionalized

phosphine ligand. The aliphatic region is dominated by three and four major signals,

respectively, which are assigned to the hydrocarbon chain of the co-condensate. In the case of

the hybrid polymers **X2b**, **X3b**, and **X3d** all main signals can be traced back to the backbone

of the matrix. It is noteworthy, that the signal occurring at about 155 ppm in each ^{13}C

CP/MAS NMR spectrum is attributed to the urea function in the spacer. The weak or missing

peaks for the alkoxysilyl substituent indicate a rather high degree of hydrolysis.

2.1.5. Hydroformylation of 1-Hexene in the Interphase

Square-planar rhodium(I) complexes have been applied as catalysts for the hydroformylation of various olefins for more than three decades [42-44]. In this work the polysiloxane-bound rhodium(I) complexes **X3a**, **X3b**, **X3c**, and **X3d** were employed in the hydroformylation of 1-hexene with good turnover numbers (TON) in dichloromethane and toluene as solvents (Tables 4 and 5). In the case of dichloromethane a complete listing of the constituents of the reaction solution is presented in Figure 3. Methanol, the most commonly solvent for catalytic hydroformylations, leads only to acetalyzation products when the above-mentioned catalysts were used, which could be demonstrated by ^{1}H and ^{13}C{^{1}H} NMR spectroscopy. It is remarkable, that the catalytic activity in toluene is higher than in dichloromethane. In the case of toluene a conversion of 1-hexene of 100 % for the first run of each catalyst was achieved. This is in contrast to the swelling capabilities of the polymers in each solvent [45]. The selectivity does not change remarkably and is 0.62 ($\pm$ 0.1) ($n/[n + iso]$) for all stationary phases. However, it was not the target of these investigations to get high yields of linear aldehyds with the simple and unspecific square-planar rhodium(I) complex.
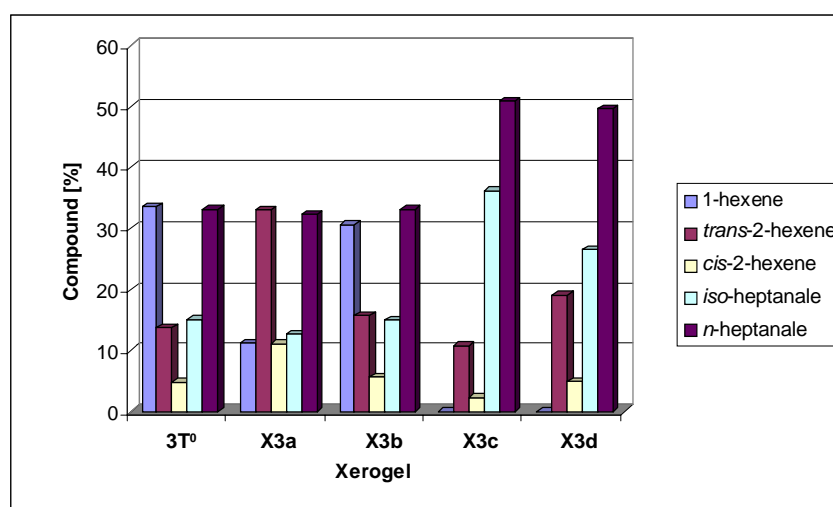
Figure 3. Composition of the solution after hydroformylation of 1-hexene in dichloromethane.

Table 4

Hydroformylation of 1–hexene in toluene [a]

Catalyst	Conversion [%]	Isomerization [%]	Hydroformylation [%]	$n/(n + iso)$	TON [b]	TOF [c]
3(T⁰)	100	17.4	82.6	0.57	13216	777
X3a	100	33.7	66.3	0.67	10608	624
X3b	100	20.9	79.1	0.58	12656	734
X3c	100	5.3	94.7	0.53	15152	891
X3d	100	7.5	92.5	0.53	14800	870

Table 5

Hydroformylation of 1–hexene in dichloromethane [a]

Catalysts	Conversion [%]	Isomerization [%]	Hydroformylation [%]	$n/(n + iso)$	TON [b]	TOF [c]
3(T⁰)	66.5	27.7	72.3	0.69	7696	452
X3a	88.9	49.5	50.5	0.72	7184	423
X3b	69.3	30.7	69.3	0.69	7680	451
X3c	100	13.0	87.0	0.58	13920	819
X3d	100	23.9	76.1	0.65	12176	716

[a] Reaction conditions: 70°C, 30 bar CO, 30 bar H_2, 1020 min, 30 ml solvent, 10 ml (80 mmol) 1-hexene, 5 μmol catalyst, ratio catalyst/substrate 1:16000. [b] Turnover number: [mol (aldehyde) / mol (catalyst)]. [c] Turnover frequency: {mol (aldehyde) / [mol (catalyst) / h]}.

A remarkable influence of the TON´s by a modification of the organic part from pure alkyl (**X3a**, **X3c)** to a chain with a phenylene unit (**X3b**, **X3d**) could not be observed. These results are in agreement with the NMR studies of the mobility of the pure polymers [45]. By variation of the silyl functionality in the co-condensation agents higher conversions, in particular in the case of dichloromethane could be detected. Co-condensation agents with T-silyl groups (**X3c**, **X3d**) show a higher catalytic activity than those, which are provided with D-silyl moieties (**X3a**, **X3b**). This result indicates that a higher cross-linkage of the polymer does not exert a negative influence on the accessibility of the reactive centers in the interphase at the described catalytic conditions. The lower mobility of the T-silyl functionalized co-condensation agents, which was observed by solid-state and suspension NMR investigations [45], and the swelling capability of the polymers, are evidently not the significant criterions for the catalytic activity of the reactive centers. A comparison of similar D- and T-silyl bifunctionalized hybrid materials in the time domain of the NMR spectroscopy is probably unsuitable. Better comparable are results of mobility studies, which were derived by dynamic fluorescence spectroscopy [46]. These investigations revealed, that polymers with the co-condensation agent **4(T^0)**, which include a fluorescence active fluorene molecule, possess a higher rotational mobility of fluorene than polymers made of **3(T^0)** in the time domain of the fluorescence spectroscopy.

Finally it is noteworthy that no leaching of the transition metal was detectable by atomic absorption spectroscopy.

2.1.6. Conclusion

A novel T-silyl functionalized triphenylphosphine (**2T^0**) was prepared by a simple coupling reaction of (*p*-aminophenyl)diphenylphosphine (**1**) and 3-triethoxysilylpropylisocyanate. Treatment of the modified phosphine **2T^0** with [μ-ClRh(CO)$_2$] gave the T-silyl functionalized rhodium(I) complex **3T^0**. After sol-gel processing with different co-condensation agents the polymers were used in the hydroformylation of 1-hexene. Although the urea function in the spacer unit can represent a different possible reactive center, there was no evidence of disadvantage in the application of these kinds of materials in catalysis. For organometallic reactions in interphases with substrates that attack the urea unit (e.g. methyliodide) the ligand has to be changed into a system without any further functional group in the spacer unit [47].

With the application of different D- and T-silyl bifunctionalized co-condensation agents in the hydroformylation of 1-hexene these various stationary phases could be directly compared for the first time under catalytic conditions. Altogether a higher cross-linkage of polymers, which are provided with T-silyl bifunctionalized copolycondensates, is more advantageous under a pressure of 60 bar. The D-silyl bifunctionalized siloxanes, which are more mobile on the NMR time scale show a lower activity under these medium pressure conditions. Properties like the swelling capability and the mobility of the different parts of the polymer become less important. The accessibility of the reactive centers and thus the catalytic activity increase with the more rigid polymer backbone of T-silyl bifunctionalized co-condensation agents under the described conditions.

2. 2. A General Synthetic Route for the Synthesis of Mono-T-Silyl Functionalized Aromatic Phosphines as Ligands for Chemistry in Interphases

2.2.1. Introduction

In this part of the thesis the synthesis of a sol-gel processable triphenylphosphine system without heteroatoms in the spacer unit is described. In contrast to the urea groups in $2(T^0)$ a further possible reactive center is eliminated. The triphenylphosphine ligand $(C_6H_5)_2PC_6H_4(CH_2)_4Si(OCH_3)_3$ $10(T^0)$ being provided with a T-silyl functionalized $(CH_2)_4$ spacer in *para*-position of only one aryl ring is obtained. by a simple four-step reaction starting with *p*-bromobutenylbenzene **6** (Scheme 3). **6** is hydrosilylated with $HSiCl_3$ to the silyl species **7** in which the chlorine atoms are exchanged by O*i*Pr groups to give $8(T^0)$. P-C coupling of $8(T^0)$ with Ph_2PCl succeeds with a Grignard reaction. Finally the O*i*Pr functions in the resulting phosphine $9(T^0)$ are replaced by OMe substituents with methanol in the presence of $CH_3C_6H_4SO_3H$. Treatment of the modified phosphine $10(T^0)$ with [μ-ClRh(CO)_2]_2 gave the T-silyl functionalized rhodium(I) complex $11(T^0)$ which is a suitable precursor for sol-gel processing.

2.2.2. Synthesis and Characterization of the T-Silyl Functionalized Triphenylphosphine Ligand 10(T⁰) and Rhodium(I) Complex 11(T⁰)

The synthesis of the T-silyl functionalized phosphine **10(T^0)** starts with the aromatically substituted olefin **6**, which is hydrosilylated by $HSiCl_3$ in the presence of the catalyst H_2PtCl_6 to give the trichlorosilylated derivate **7** (Scheme 3). It is not necessary to isolate **7**. In a subsequent reaction the crude liquid **7** is treated with triisopropyl orthoformate at ambient temperature. Under these very mild conditions the chlorine atoms are exchanged quantitatively by O*i*Pr groups. The presence of O*i*Pr residues in **8(T^0)** is a necessary precondition for a successful Grignard reaction with the aryl bromide **8(T^0)**. After the addition of magnesium the reaction mixture has to be cooled to –20°C to avoid the formation of tetraphenyldiphosphine. Because hydrolysis of crude **9(T^0)** is not possible, it has to be extracted with *n*-pentane to give the coupling product **9(T^0)** in good yields. To accelerate the sol-gel process, finally the O*i*Pr groups were replaced by OMe. The T-silyl functionalized triphenylphosphine **10(T^0)** is obtained as a bright yellow oil, which is sensitive to moisture and air and dissolves readily in all common organic solvents.

A similar phosphine ligand with a triethoxysilyl function has been published 25 years ago [48]. However, the authors did not report on any spectral data and it was not possible to reproduce the synthetic procedure.

Both intermediates **8**, **9(T^0)** were characterized by EI mass spectrometry, ^1H, $^{13}C\{^1H\}$, $^{29}Si\{^1H\}$, and $^{31}P\{^1H\}$ spectroscopy, and elemental analyses (see Experimental section). The composition of the trimethoxysilyl functionalized phosphine 5(T^0) was corroborated by its EI mass spectrum showing the molecular peak at $m/z = 438$. In the $^{31}P\{^1H\}$ and $^{29}Si\{^1H\}$ NMR spectra of **10(T^0)** each one signal is observed at $\delta = -5.02$ and -41.3, respectively. Compared to triphenylphosphine the *para*-positioned spacer function exerts nearly no influence on the

Br

$HSiCl_3$

H_2PtCl_6

Br

$SiCl_3$

$HC(OiPr)_3$

Br

$Si(OiPr)_3$

6   **7**   **8(T^0)**

1.) Mg
2.) Ph_2PCl

(THF)

$Si(OiPr)_3$

MeOH

$CH_3C_6H_4SO_3H$

$Si(OMe)_3$

9(T^0)   **10(T^0)**

$[\mu\text{-ClRh(CO)}_2]_2$

Ph$_2$
P/ /Rh\\CO
Cl◄   ►P
Ph$_2$

$(MeO)_3Si$—

11(T^0)

—$Si(OMe)_3$

Scheme 3.
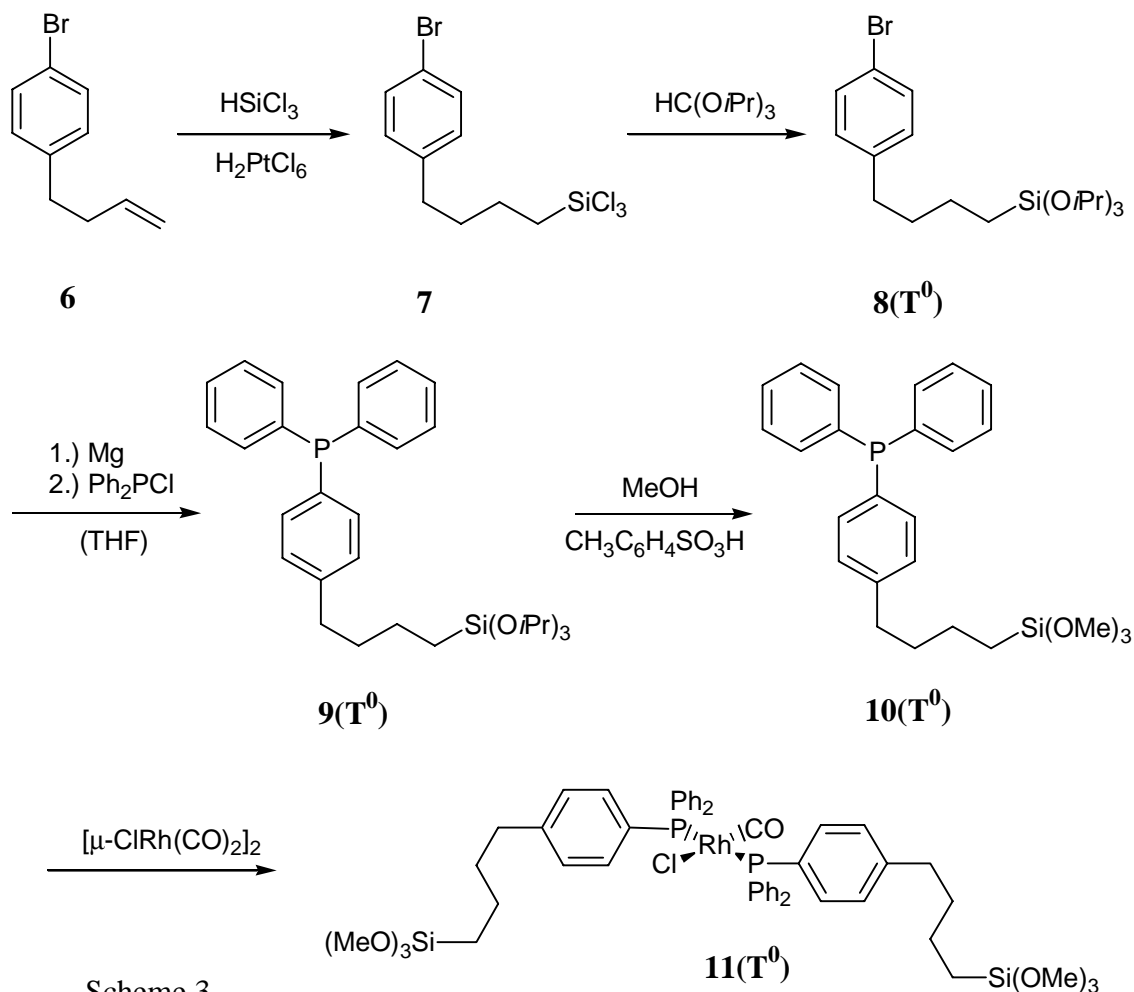
chemical shift of the ^{31}P nucleus in **10(T^0)**. The completeness of the exchange of the O*i*Pr

groups by OMe residues can be monitored by ^{1}H and ^{13}C{^{1}H} NMR spectroscopy.

Since phosphinerhodium(I) complexes play an important role as catalysts in the

hydroformylation of olefins the modified triphenylphosphine **10(T^0)** was reacted with [μ-

ClRh(CO)$_2$]$_2$ in CH$_2$Cl$_2$. After evaporation of the solvent a yellow waxy product is obtained

which proved to be the T-silyl functionalized rhodium(I) complex **11(T^0)**.

Only one doublet with a ^1J(RhP) coupling constant of 126.2 Hz occurs in the ^{31}P{^{1}H}

NMR spectrum of complex **11(T^0)**, which is indicative of a *trans*-position of the phosphine

ligands (Figure 4). A characteristic absorption at 1974 cm^{-1} in the IR spectrum of **11(T^0)** is

assigned to the carbonyl stretching vibration. Other analytic data are summarized in the

experimental section.
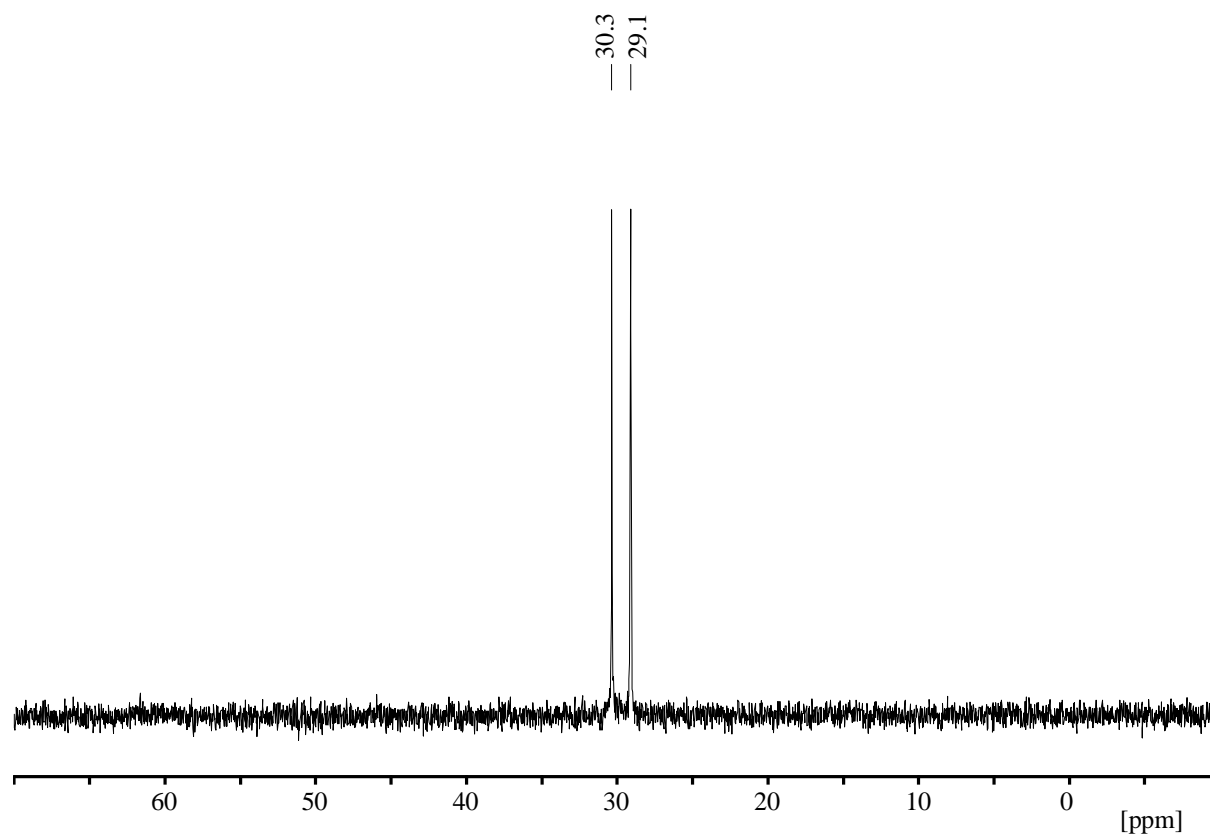
Figure 4. $^{31}P\{^1H\}$ NMR spectrum of **11(T^0)**.

2.2.3. Conclusion

It is of great advantage that it is possible to generalize the synthetic route for the T-silyl functionalized phosphine **10(T^0)** presented in Scheme 3. Not only the spacer length can be varied by the employment of different alkenylbenzenes of the type 1, it is also conceivable to incorporate other phosphorus attached substituents, if in the case of the Grignard reaction step other chlorodiorganylphosphines are used. In addition the availability of the modified triphenylphosphine **10(T^0)** and the rhodium(I) complex **11(T^0)** allows to compare reactions in interphases with those of the corresponding triphenylphosphinerhodium(I) complex in homogeneous phase.

2. 3. Accessibility Studies of Sol-Gel Processed Phosphane-Substituted Iridium(I) Complexes in the Interphase

2.3.1. Introduction

A major intrinsic intricacy that may occur in reactions in interphases are diffusion problems which adversely influence the activity of the catalysts. All reactive centers should be readily accessible for substrates. Excellent model systems for accessibility studies represent iridium complexes which are much more stable compared to corresponding rhodium congeners. The objective of this work was the performance of organometallic model reactions
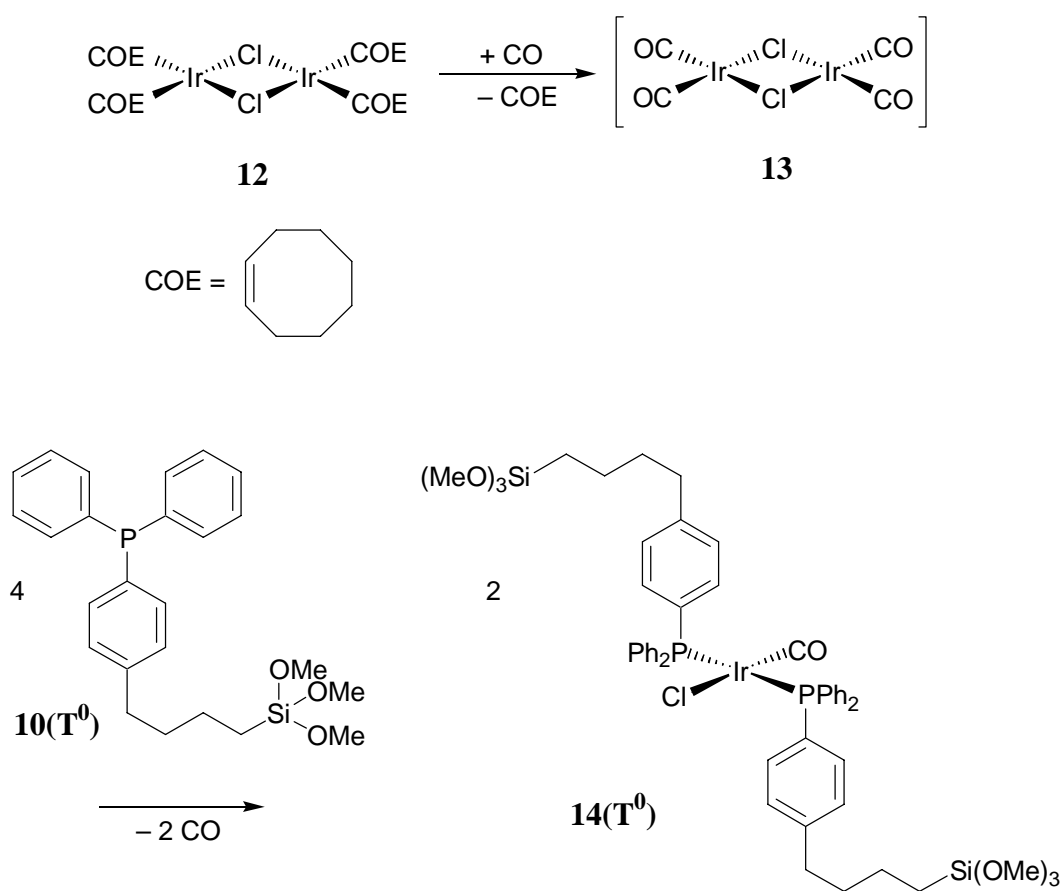
Scheme 4.

in interphases. Therefore the reactive behavior of an iridium(I) complex incorporated into a stationary phase was examined towards a series of molecules with different shapes and sizes like oxygen, sulfur dioxide, dicyanoethyne, and different halogenated substrates. The resulting products were characterized by several spectroscopic methods as well as by EXAFS and EDX.

2.3.2. Sol-Gel Processing of the Monomeric Iridium(I) Precursor Complex 14(T^0)

The iridium(I) complex **14(T^0)** was obtained by a modification of the synthetic pathway of Roberto et al. (Scheme 4) [49]. A stoichiometric amount of the T-silyl functionalized phosphane ligand **10(T^0)** [47] was added to an acetonitrile solution of [μ-ClIr(CO)$_2$]$_2$ (**13**) to give a light brown solution of **14(T^0)** which was directly subjected to the sol-gel process. A single peak in the ^{31}P{^{1}H} NMR spectrum of **14(T^0)** at $\delta = 24.7$ and one $\tilde{v}$ = (CO) absorption in the IR spectrum at 1966 cm^{-1} indicate the completeness of the reaction [50, 51].

A molar 1:5 mixture of the iridium complex **14(T^0)** and of the co-condensation agent **5(T^0)** [45] was hydrolyzed and polycondensed in water/THF in the presence of tetrabutylammoniumfluoride (TBAF) as catalyst at room temperature (Scheme 5).
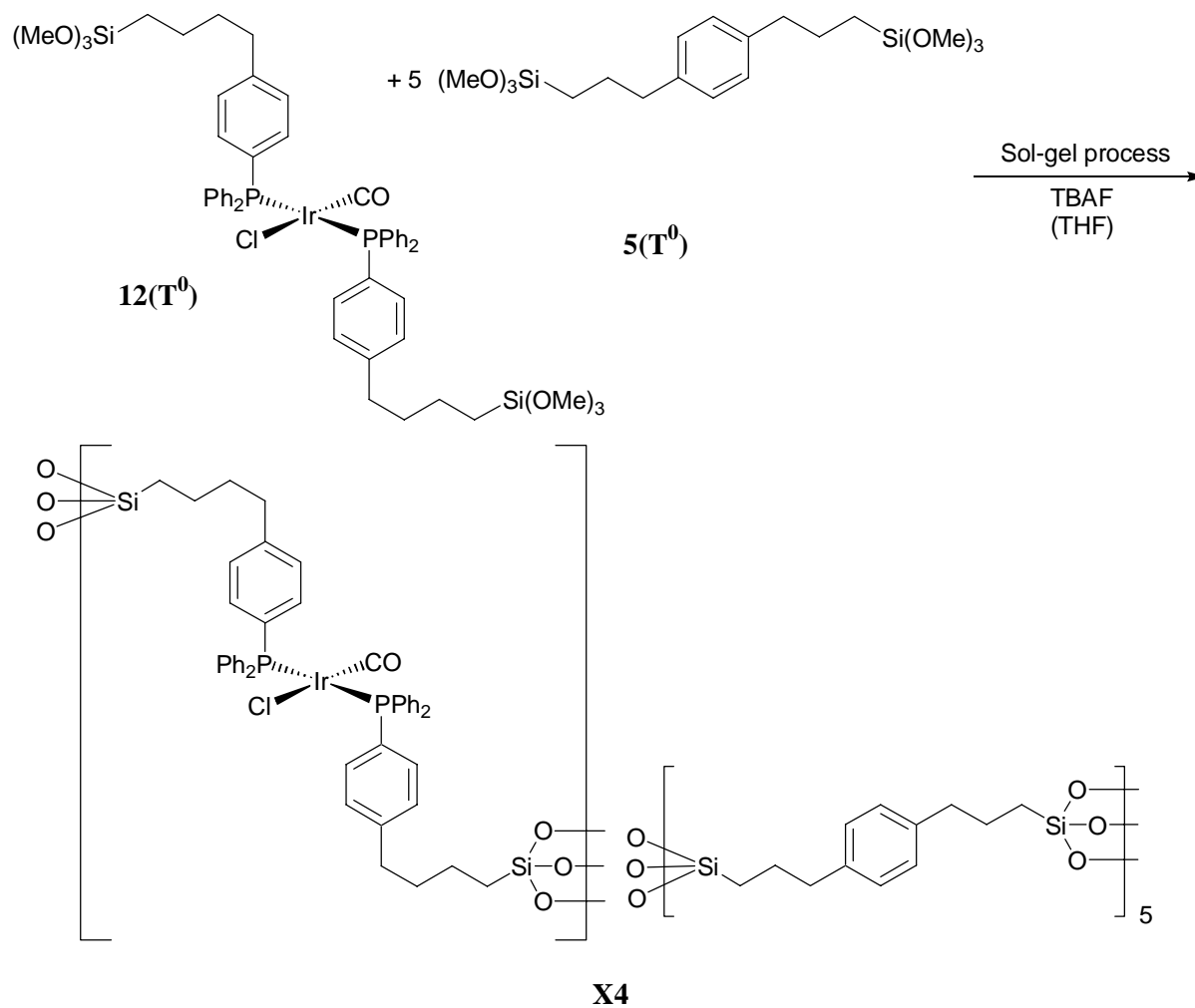
Scheme 5.

Idealized polycondensation: **13[12(T³)][5(T³)]₅**

Realistic composition: **13[12(Tⁿ)][5(Tⁿ)]₅ (X4)**

T = T type of silicon atom (three oxygen neighbours)
n = numbers of Si-O-Si bonds (n = 0-3)

Scheme 6.
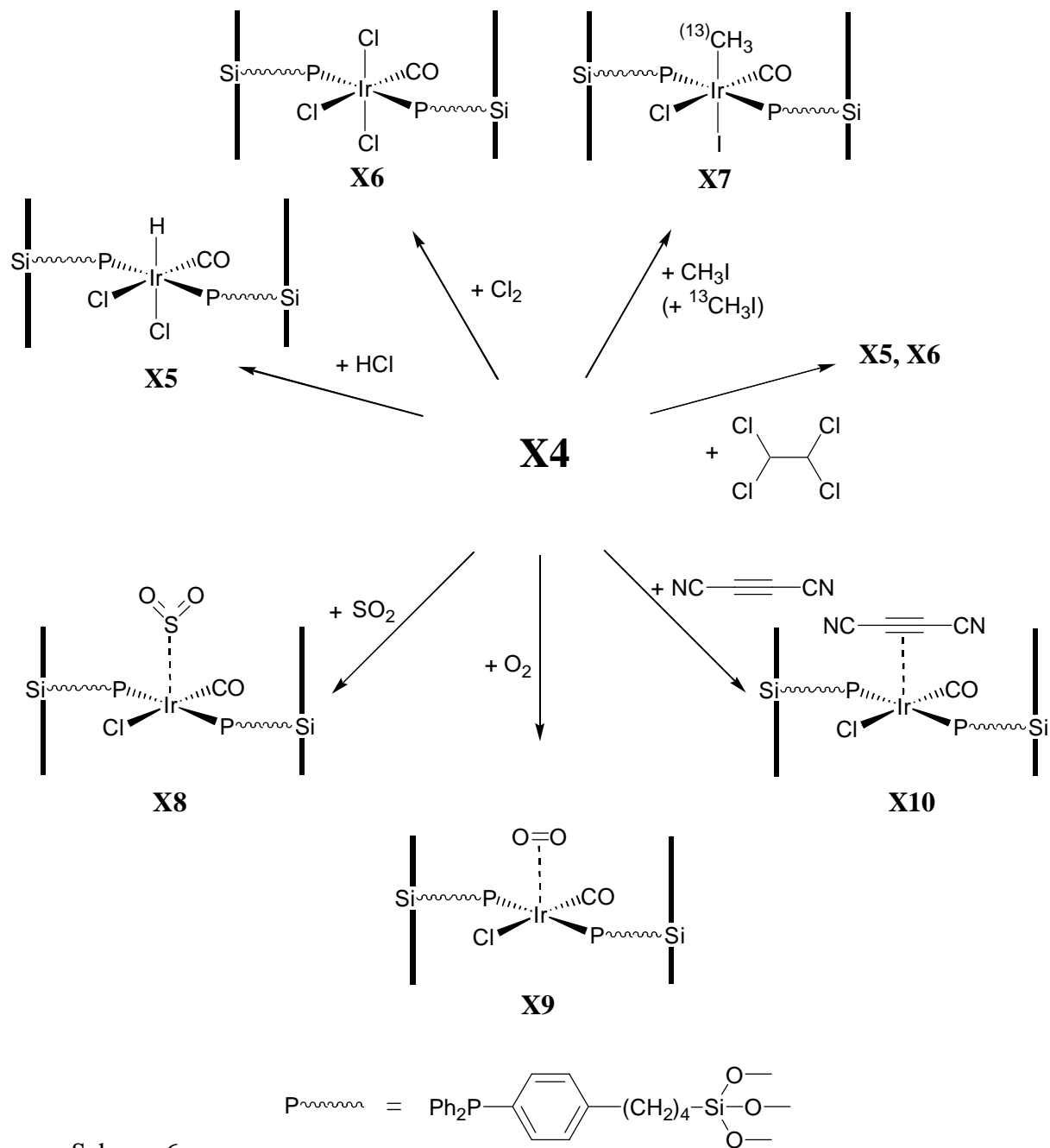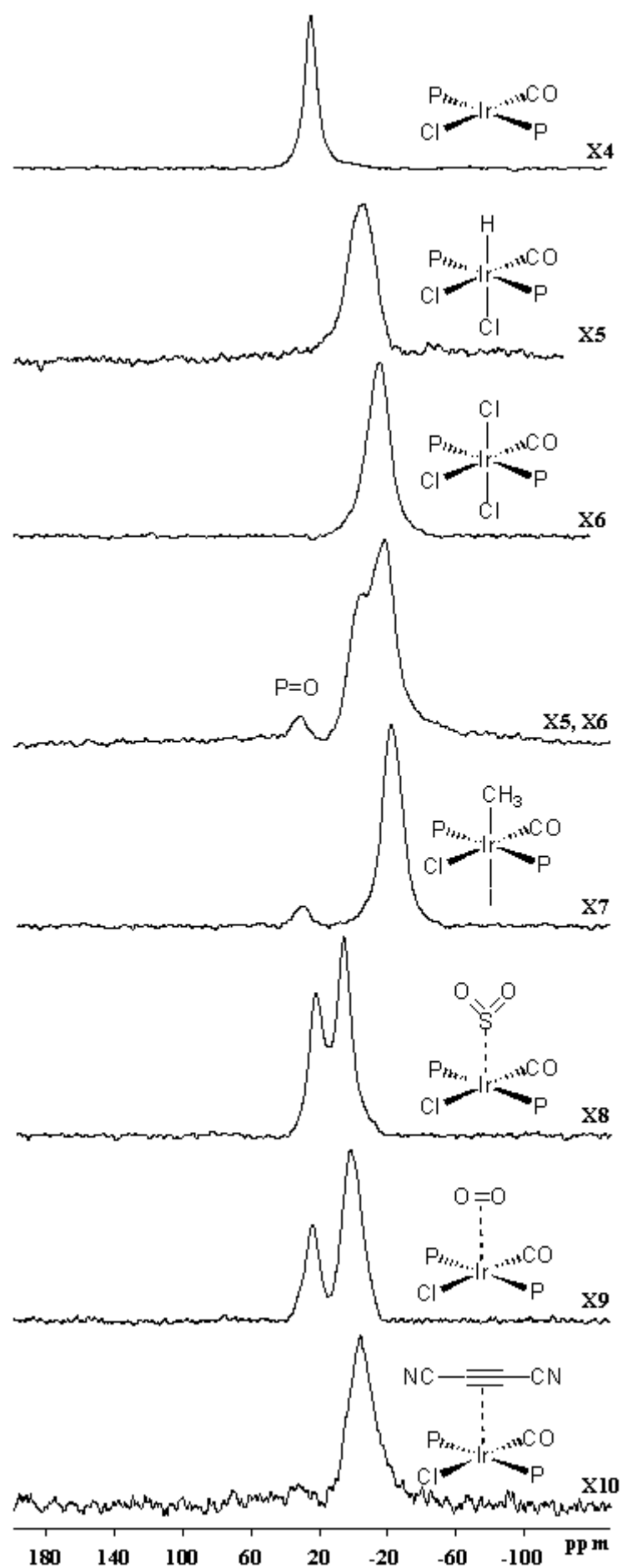
Figure 5. ^{31}P CP/MAS NMR spectra of the xerogels **X4-X10**.

The resulting xerogel **X4** represents a pale yellow powder which is rather air stable. In the [31]P

CP/MAS NMR spectrum of the polysiloxane–bound iridium(I) complex   **X4** only one signal is

observed with a chemical shift of δ = 24.4, which is in agreement with the monomeric

complex **14(T^0)** measured in solution (Figure 5). To decide whether the phosphanes in **X4** are
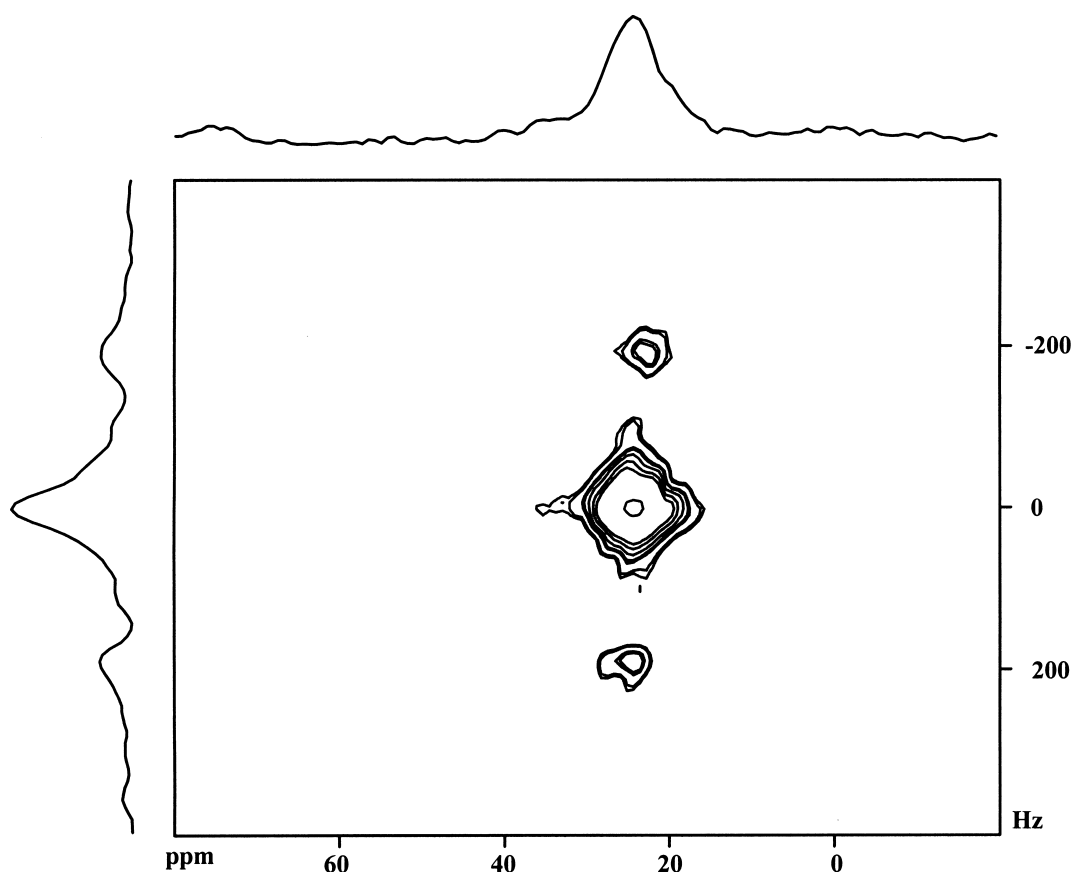
Figure 6. *J*-resolved 2D ^{31}P CP/MAS NMR spectrum of **X4**.

cis or *trans* oriented to each other a according to a phase-cycled spin-echo-experiment was

recorded (Figure 6) [52]. The $^2J_{PP}$ coupling constant of approximately 400 Hz is consistent

with a *trans* configuration. In the ^{13}C CP/MAS NMR spectrum of **X4** all main signals stem

from the co-condensing moiety. The missing signal for the Si–OMe function indicates a high

degree of hydrolysis. All silicon atoms in the polysiloxane matrix are in direct proximity of
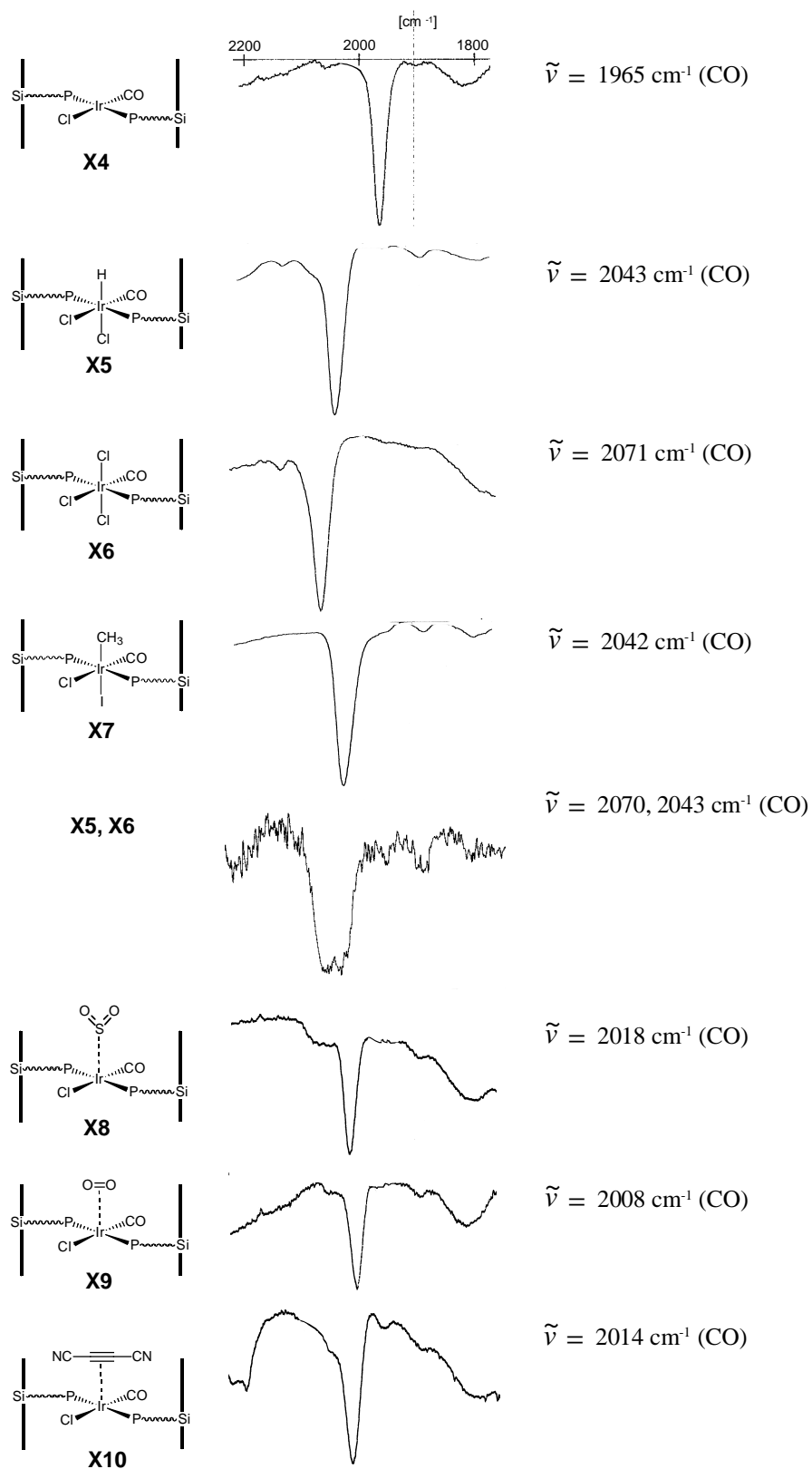
Figure 7. IR spectra of the xerogels **X4**-**X10**.

protons, thus silyl species are detectable via cross polarization. The signals in the ^{29}Si

CP/MAS NMR spectrum of the copolymer **X4** are located in the typical range for T–silyl

functions and their substructures   T^2–T^3 [δ = − 57.3 (T^2), − 65.7 (T^3)]. The degree of

condensation, which was determined by generally known methods [5354], is 87 %. Spin–

lattice relaxation times of the protons in the rotating frame ($T_{1\rho H}$) were determined by a direct

spin lock–τ–CP experiment [55] via ^{29}Si and ^{31}P. In all cases the observed decays of the

magnetization were monoexponential. Thus the relaxation mechanism is spin–diffusion

controlled and the material is considered as homogenous. The formation of domains larger

than 1 – 2 nm in diameter is excluded.

The $\tilde{v}$ (C≡O) vibration (1965 cm^{-1}) in the IR spectrum of **X4** is comparable to that one

of **14(T^0)** in solution (Figure 7). The elemental composition of the stationary phase **X4** was

determined by EDX (Table 6).

2.3.3. Oxidative Addition Reactions on the Stationary Phase X4 with Hydrogen Chloride, Chlorine, Tetrachloroethane, and Methyliodide (^{13}C-Methyliodide)

Treatment of the solid **X4** with hydrogen chloride and chlorine (interphase system

solid/gaseous) lead to a color change from yellow to white and the polymer-anchored iridium

complexes **X5** and **X6** were quantitatively formed. The ^{31}P CP/MAS NMR and IR spectra are

in full agreement with the data recorded for the corresponding monomeric complexes in

solution (see Experimental Part and Figures 5 and 7) [56].

In the case of the reaction between **X4** and tetrachloroethane in benzene (interphase

system solid/liquid) a mixture of two different products was obtained. One component proved

to be the meridional trichloroiridium(III) complex **X6** the monomeric congener of which has

Table 6

Elemental analysis of compounds **X4-X7** by EDX. Hydrogen cannot be measured by X-ray emission spectroscopy. Therefore, the reference data have been renormalized excluding hydrogen

| Xerogel | Reference data [a] | | | | | | | EDX [b] | | | | | | |
| | Composition [%] | | | | | | | Composition [%] | | | | | | |
	C	O	Si	P	Cl	Ir	I	C	O	Si	P	Cl	Ir	I
X4	57.54	13.87	15.38	2.83	1.62	8.77	---	59.33	15.54	13.87	2.60	1.19	7.47	---
X5	56.62	13.65	15.13	2.78	3.18	8.63	---	56.59	11.16	17.77	3.51	2.89	8.08	---
X6	55.74	13.43	14.89	2.74	4.70	8.50	---	58.78	14.58	13.14	3.18	4.76	5.56	---
X7	54.63	13.04	14.46	2.66	1.52	8.25	5.44	54.55	13.37	14.89	2.97	1.14	8.57	4.50

[a] Calculated from theory. Complete condensation was assumed. [b] Quantified by the ZAF correction procedure.

been described in an earlier work by Al-Najjar [57]. Interestingly the second species turned out to be complex **X5**, already mentioned when hydrogen chloride was oxidatively added to **X4**. Obviously not only a C–Cl, but also a C–H activation has taken place already at room temperature in a competitive reaction path. The ^{31}P CP/MAS NMR spectrum reveals two resonances at $\delta = -3.0$ (**X5**) and -18.2 (**X6**) (Figure 5). An unresolved broad absorption in the C≡O region between 2030 and 2080 cm^{-1} was found in the IR spectrum of this mixture (Figure 7). A direct comparison of these results with those of the known monomeric iridium(III) complexes [56] confirms the adopted structures depicted in Scheme 6.

Also methyl iodide could be oxidatively added in benzene to the iridium complex in
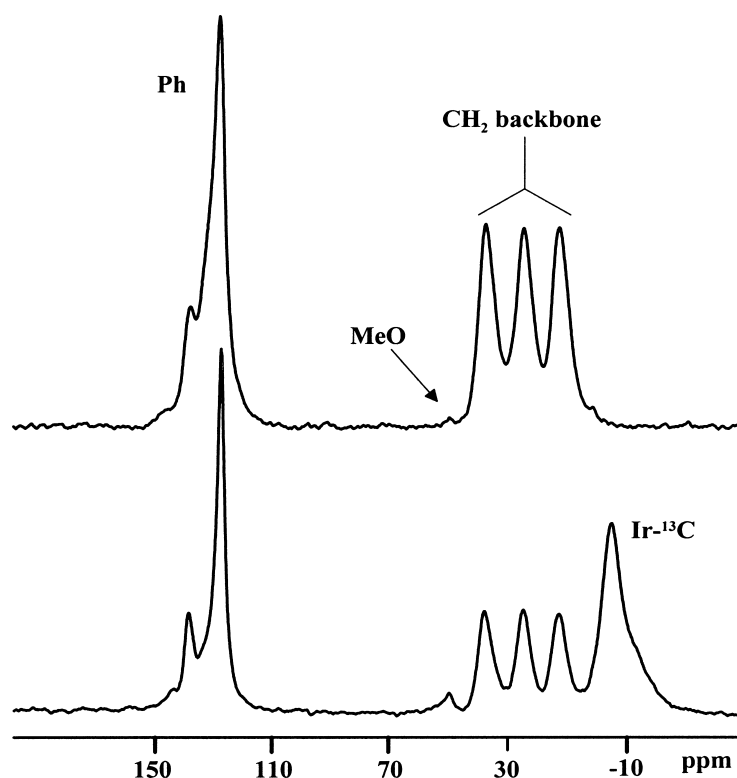
Figure 8. ^{13}C CP/MAS NMR spectra of the stationary phase **X7** (top: without ^{13}C labeling of the methyl iridium group; bottom: with ^{13}C labeling of the methyl iridium group).

X4 in the interphase (solid/liquid) to give the air-stable light brown polymer **X7** (Scheme 6). The carbonyl ligand gives rise to a strong absorption band at 2042 cm^{-1} which is in accordance with the literature for the corresponding monomeric complex in solution [58]. Only one resonance is observed in the ^{31}P CP/MAS NMR of **X7** (Figure 5) indicating a complete conversion of the reaction. If ^{13}C labeled methyl iodide was applied an additional intense signal was observed in the ^{13}C CP/MAS NMR spectrum, which is consistent with an iridium-bound methyl group (Figure 8).

2.3.4. Reactions of the Stationary Phase X4 with Sulfur Dioxide, Oxygen, and Dicyanoethyne

In the interphase systems solid/gaseous and solid/liquid the polysiloxane-bound iridium(I) complex **X4** was reacted with sulfur dioxide, oxygen, and dicyanoethyne to give the polymeric products **X8**, **X9**, and **X10** (Scheme 6). The C≡O stretching vibration in the IR spectra of these materials corroborated a complete conversion. Absorptions at 2018, 2008, and 2014 cm^{-1} (Figure 7) were observed which are shifted to higher wave numbers compared to **X4** (1966 cm^{-1}). These spectra were recorded in a sulfur dioxide (**X8**) and oxygen (**X9**) atmosphere, respectively. However, the ^{31}P CP/MAS NMR spectra of **X8** and **X9** reveal two ^{31}P resonances (Figure 5). Since the rotors could only be packed without an oxygen and sulfur dioxide atmosphere a reversible reaction took place resulting in a partial formation of the starting material **X4**. In contrast to this observation the dicyanoethyneiridium(I) complex **X10** shows only one ^{31}P signal at $\delta = -3.3$ (Figure 5). These findings are in agreement with literature data [59] for the monomeric congeners in which oxygen, dicyanoethyne, and sulfur dioxide are η^2- and η^1-coordinated, respectively.

2.3.5. EXAFS and EDX Measurements of Selected Stationary Phases

One of the most powerful methods to obtain interatomic distances of amorphous materials is the extended X-ray absorption fine structure spectroscopy (EXAFS). The xerogel **X7** was chosen as an example to determine the bond lengths between the metal center and the coordinating atoms of the ligand. The k^3 weighted EXAFS function (Figure 9a) of **X7** can be described best by six different atom shells. The first intensive peak in the corresponding Fourier transform (Figure 9b) is mainly due to the carbon atoms. Chlorine and phosphorus atoms were found in the case of the most intense peak, and the third intense peak belongs to the iodine and oxygen atoms. For the most intense peak of the Fourier Transform (Figure 9b), two equivalent phosphorus atoms and one chlorine atom with Ir-P and Ir-Cl bond distances of
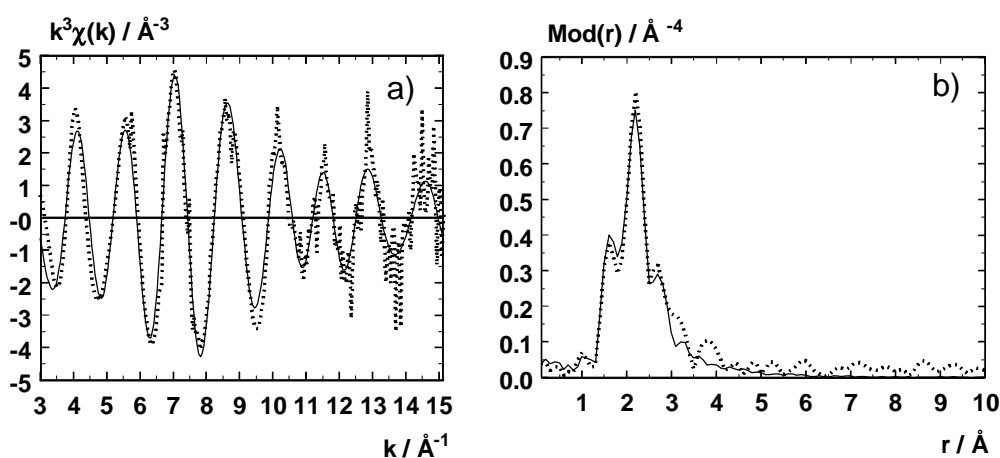
Figure 9. Experimental (dotted line) and calculated (solid line) $k^3\chi$ (k) functions (**a**) (k range: 2.99 – 15.14 Å^{-1}) and their Fourier transforms (**b**) for **X4** (Ir- L_3-edge) (see Table 2 for fit parameter).

2.40 and 2.46 Å, respectively, were found. These results reveal a good agreement between the experimental and the calculated functions. A significant improvement in the fit of the first intense peak was obtained, if two carbon atoms with Ir-C1 (Ir-CO bond) and Ir-C2 (Ir-CH$_3$)

bond distances of 1.86 and 2.19 Å, respectively, are considered (Figure 9b). Additionally each

one iodine and oxygen atom with an Ir-I bond length and an Ir-O distance of 2.63 and 3.08 Å

were detected, leading to an improvement of 7.4 and 18.9 % in the fit, respectively.

Interatomic distances of **X7** which is consistent with crystal structures of similar iridium(III)

complexes like $IrCl_3(CO)(PPh_3)_2$ [60], $IrCl(H)(SH)CO(PPh_3)_2$ [61], and $[Ir(OClO_3)(CH_3)$

$(H_2O)(CO)(PPh_3)_2]ClO_4$ [62] are summarized in Table 7.

Table 7

EXAFS-determined structural data of **X4**

	N [a]	r [Å] [b]	σ [Å] [c]
Ir–C1 (CO) [d]	1	1.86 ± 0.02	0.050 ± 0.005
Ir–C2 (CH$_3$) [d]	1	2.19 ± 0.02	0.095 ± 0.010
Ir–P [d]	2	2.40 ± 0.02	0.067 ± 0.010
Ir–Cl [d]	1	2.46 ± 0.03	0.097 ± 0.010
Ir–I [d]	1	2.63 ± 0.03	0.118 ± 0.012
Ir–O [d]	1	3.08 ± 0.03	0.050 ± 0.005

[a] Coordination number N. [b] Interatomic distance r. [c] Debye-Waller factor σ. [d] Absorber-backscatterer.

Typical EDX spectra of compounds **X6** and **X7** are displayed in Figure 10. The K_α

lines of carbon, oxygen, silicon, phosphorus, and chlorine and the L_α line of iridium are
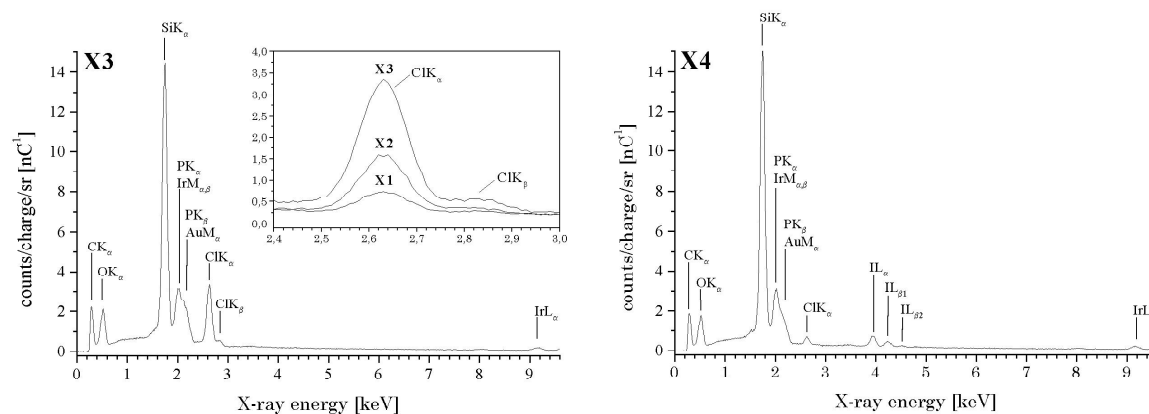
Figure 10. Energy dispersive X-ray spectra of compounds **X6** (left) and **X7** (right). As shown by comparison of the ClK$_\alpha$ emission line intensities in the inlay, the chlorine content clearly increases from **X4**-**X6**. Quantification results are summarized in Table 6.

clearly visible. The M$_\alpha$ and M$_\beta$ lines of iridium are overlapped by the K$_\alpha$ peak of phosphorus. In the case of **X7**, the L line series of iodine also appears in the spectrum. The increasing content of chlorine in the xerogels **X4**-**X6** is evident as the intensity of the chlorine K line emission increases in the same direction.

Quantification of EDX spectra was carried out using the ZAF correction procedure. The ZAF correction procedure is valid only for flat specimens. As the xerogels exhibit a pronounced morphology (Figure 11) special care was taken to find a locally flat specimen area larger than the expected electron range which is certainly below 10 µm under the present conditions. Other sources of error, especially in light element analysis, are uncertainties in fundamental parameters and spectrometer calibration at X-ray energies below 1 keV. Spectral interferences occurring between iridium and phosphorus can be corrected by peak deconvolution. Due to its high fluorescence yield, the Au M$_\alpha$ line also appears under the K$_\beta$ emission of phosphorus. However, the gold coating can be neglected with respect to quantification as owing to its thickness of only 20 nm additional absorption effects are not introduced.
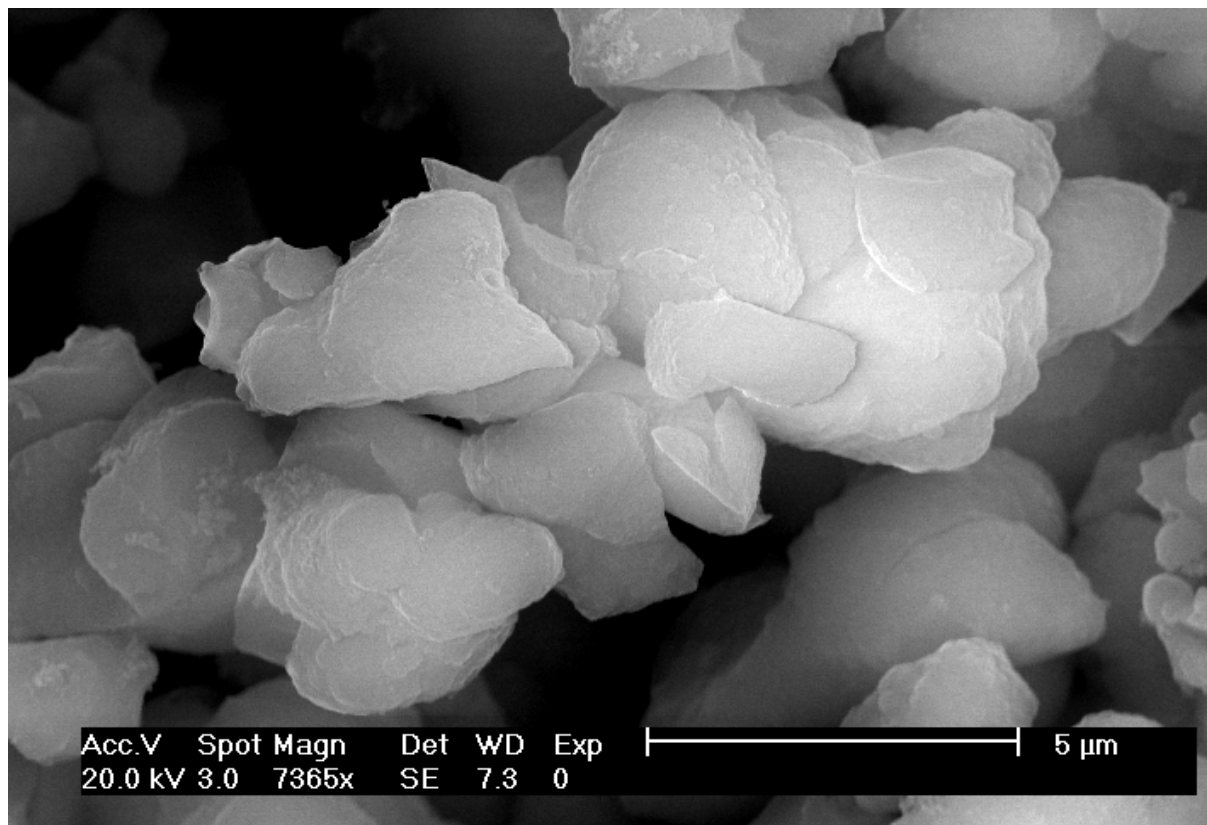
Figure 11. Scanning electron micrograph of **X4**.

Despite the numerous sources of error simultaneous quantification of all present elements was carried out successfully. The elemental analyses by EDX are summarized in Table 6 and compared to data obtained from solid state NMR measurements. These have been renormalized excluding hydrogen as a single-electron atom does not emit characteristic X-rays. Except for the iridium content in xerogel **X6** the elemental analyses support the reference data within the limits of error with the given samples.

2.3.6. Conclusion

For successfully catalytic processes in interphases the polysiloxane-bound reactive centers should be completely accessible for substrate molecules. Therefore catalytic model reactions, for example the activation of small and larger molecules, are of great importance for the better understanding of catalytic reactions in interphases. To introduce reactive centers a phosphaneiridium(I) complex has been chosen, because such a system is suitable for the envisaged model reactions. For the construction of a mobile stationary phase the T-silyl functionalized iridium complex **14(T^0)** was co-polycondensed with the bifunctionalized co-condensation agent $(MeO)_3Si(CH_2)_3C_6H_4(CH_2)_3Si(OMe)_3$ [**5(T^0)**] which has been already successfully employed in the rhodium catalyzed hydroformylation of 1-hexene. The iridium-containing xerogel **X4** was then subjected to various oxidative additions and to the coordination of an alkyne. It could be unequivocally demonstrated, that the iridium centers in **X4** were completely accessible for the mentioned substrates with different shapes and sizes. The higher cross linkage of the T-silyl bifunctionalized co-condensation agent in the hybrid polymer matrix does not exert a disadvantageous effect on the accessibility of the metal centers. This fact presents a necessary precondition for a successful catalytic process. With the examples of the reactions with sulfur dioxide and dioxygen it could be shown that substrate molecules are also able to reversibly leave the polysiloxane matrix without any interference.

Most of these model reactions were also carried out with the corresponding rhodium(I) interphase system. However, the formed complexes proved to be unstable and underwent partially decomposition.

2. 4. New Inorganic-Organic Hybrid Materials for HPLC Separation Obtained by Direct Synthesis in the Presence of a Surfactant

2.4.1. Introduction

The further development of new tailored materials for the enrichment and separation of synthetic and natural compounds plays an important role in chemical, pharmaceutical, medical, and biological research. High-performance liquid chromatography (HPLC) is currently the most commonly applied technique to separate and analyze multi-component mixtures. In this field the application of stationary phases based on silica gel is very popular due to their high pressure and pH stability. For the successful employment of silica it is of great importance, that the silica beads show a narrow particle size distribution, and that the particles have a spherical shape. Several years ago, Stoeber et al. [63] published a procedure for the access to monodisperse nonporous spherical silica particles of about 1 µm size. With the discovery of M41S materials [64,65] some time later, the development of tailor-made ordered mesoporous silicas was achieved. The conventional way to synthesize MCM-41 phases is based on the condensation of a solution of sodium silicate with an ammonium salt containing a long n-alkyl chain at a temperature of about 100°C [64]. Such a system forms micelles with the silicate anion species via a process of cooperative interaction [66]. It is possible to tune the pore size through the variation of the n-alkyl chain length of the ammonium salt and the specific surface areas of these materials are > 1000 m^2/g. However, MCM-41 is an agglomerated silica with a primary particle size of about 50 nm. Because of these properties, the materials do not resist high pressure, hence an application in HPLC is impossible [67] Tanev and Pinnavaia [68] employed n-alkylamines as templates, but they did

not obtain spherical particles. Unger et al. [69] improved this synthetic route, to get a tunable particle diameter and a nearly monodisperse particle size distribution. Recently, several investigations have been reported, in which nanostructured, mesoporous silicas were successfully applied in HPLC [70,71].

More than 60% of all HPLC separations are carried out under reversed phase (RP) conditions. The surface modification of well defined silica beads with T-silyl functionalized organic systems [72] is the major route to create phases for reversed-phase liquid chromatography (RPLC). C_8, C_{18}, and C_{30} phases were successfully employed for the separation of mixtures of aromatic compounds and carotinoids, respectively.[73,74] In RP chromatography not only long alkyl chains but also stationary phases containing aromatic selectors such as benzene, pyrene [75], fluorene [76-77], and acridine [78] have been investigated so far. However, there is still a need to develop tailored stationary phases with better extraction, enrichment and separation behavior for natural substances.

Recently, many investigations were extended to nanostructured mesoporous silica, which are based on inorganic-organic hybrid polymers [68,79-91]. These materials are provided with extremely high surface areas and accessible pores [87,25]. Moreover, the pore size can be tuned in the nanometer range by choosing template systems with different sizes or with a co-solvent. In this work, it was combined the advantages of nanostructured, mesoporous hybrid materials with long alkyl chain modified reversed-phases for HPLC. A simple one step synthetic pathway is described, which is accompanied by a high reproducibility, to get an efficient separation material by cocondensation of tetraethoxysilane (TEOS) with *n*-octyl, *n*-dodecyl, and *n*-octadecyltrialkoxysilane, respectively. All other well-known RP materials were synthesized by surface modification of silicas and need two reaction steps at least starting from TEOS.

The surface modification of silica with triacontyl chains clearly shows that a detailed characterization of molecular recognition structures is one of the essential necessities for the

development of new materials for specific applications [92-96]. Solid-State NMR spectroscopy (^{29}Si and ^{13}C CP/MAS) proved its great importance, wide range of application and its meaningfulness in the demanded of detailed structure elucidation [92,97,98]. The existence of alkyl chains of different mobility and its alignment influences the separation. This shows that the separation can be improved if the molecular recognition sites have similar structures. Brunauer-Emmett-Teller (BET) adsorption measurements were performed to fully characterize the surface area. X-ray low angle diffraction and electron diffraction experiments were carried out to determine the degree of organization within the stationary phases.

The properties of these novel hybrid materials are suitable for application in HPLC. High surface areas of $900 - 1400$ m^2/g are found which are comparable to values measured with similar materials [25]. Standard reference materials containing mixtures of polycyclic aromatic hydrocarbons (PAHs) were employed not only to characterize the new columns but also to prove the high shape selectivity of the mesoporous packing materials.

2.4.2. Synthesis of the Stationary Phases, Scanning Electron Microscopy, and Particle Size Distribution

For the access to the ordered mesoporous hybrid materials $\mathbf{X_n11}$, $\mathbf{X_n12}$, and $\mathbf{X_n13}$ (n = 9, 15, 19) a template synthesis [87,25] was necessary (Scheme 7) by modification of the known synthetic pathway of Pinnavaia et al. [68] Long alkyl chains commonly used for liquid chromatography were introduced by using the alkyltrialkoxysilanes $CH_3(CH_2)_7Si(OMe)_3$ (**15**) and $CH_3(CH_2)_ySi(OEt)_3$ [y = 11(**16**), 17(**17**)] as starting materials. In the presence of *n*-hexadecylamine as template which concomitantly serves as a catalyst, the precursors **11x**-**13x** and the cocondensation agent $Si(OEt)_4$ (TEOS) were sol-gel processed in different ratios (1:9, 1:15 , and 1:19, Table 9 and Experimental Section). A mixture of EtOH and H_2O was

employed to improve the solubility of the template. The properties of the polycondensation

products strongly depend on boundary conditions, such as concentration of the monomers,

type of solvents, temperature, reaction time, and kind of catalyst. To ensure comparable

$R \sim Si(OR')_3$ + $n\ Si(OEt)_4$

$n = 9, 15, \text{ and } 19$

15 R = C_6H_{13} R' = Me
16 R = $C_{10}H_{21}$ R' = Et
17 R = $C_{16}H_{33}$ R' = Et

$n\text{-}C_{16}H_{33}NH_2$ / $H_2O/EtOH$

$C_{15} = C_{15}H_{31}$

Extraction (EtOH) / $- n\text{-}C_{16}H_{33}NH_2$

Scheme 7.

X$_n$11
X$_n$12
X$_n$13
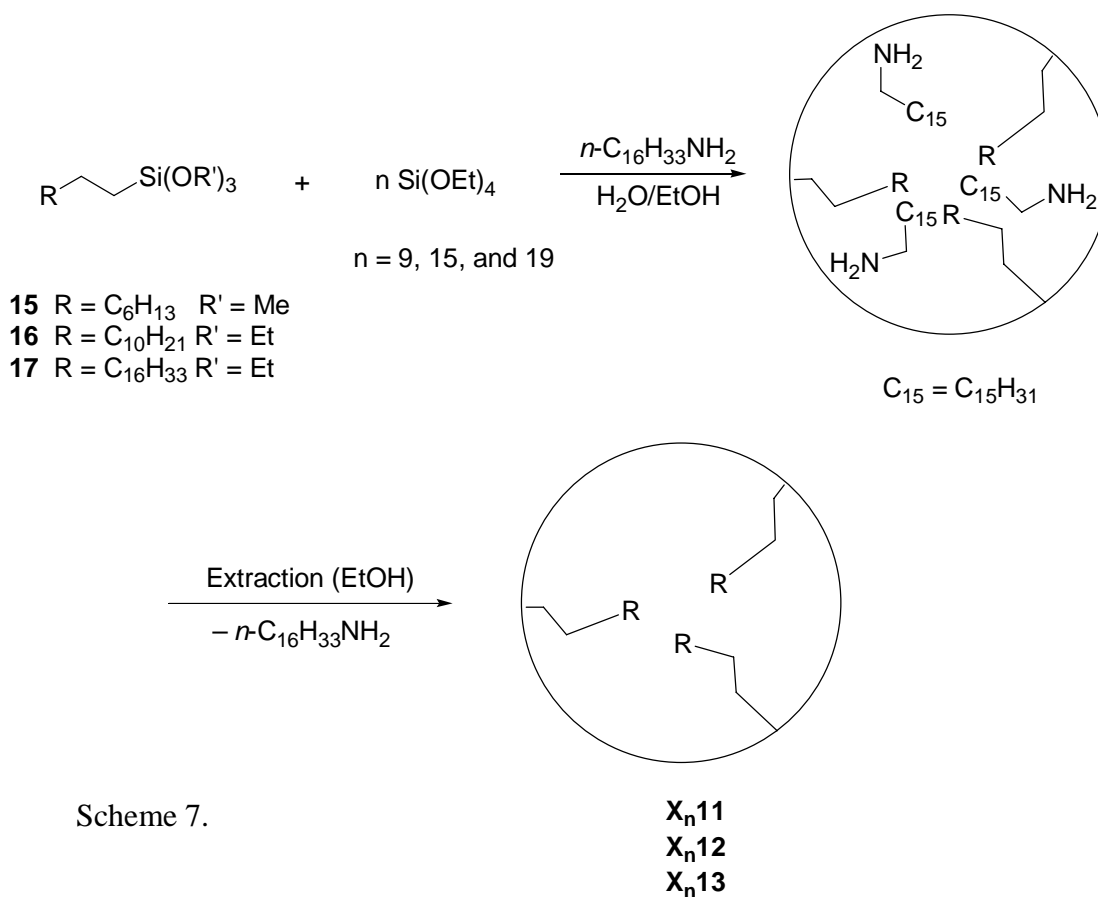
results, uniform reaction conditions throughout hydrolysis and the sol-gel transition must be

maintained. After sol-gel processing at ambient temperature the amine was removed from the

xerogels by Soxhlet extraction with ethanol.

Table 9

Sol-gel processes and labeling of the materials

Organotrialkoxysilane	Employed ratio of organotrialkoxysilane / TEOS	Xerogel
$C_8H_{17}Si(OMe)_3$ (**15**)	1 : 9	**$X_9$11**
$C_8H_{17}Si(OMe)_3$ (**15**)	1 : 15	**X_{15}11**
$C_8H_{17}Si(OMe)_3$ (**15**)	1 : 19	**X_{19}11**
$C_{12}H_{25}Si(OEt)_3$ (**16**)	1 : 9	**$X_9$12**
$C_{12}H_{25}Si(OEt)_3$ (**16**)	1 : 15	**X_{15}12**
$C_{12}H_{25}Si(OEt)_3$ (**16**)	1 : 19	**X_{19}12**
$C_{18}H_{37}Si(OEt)_3$ (**17**)	1 : 9	**$X_9$13**
$C_{18}H_{37}Si(OEt)_3$ (**17**)	1 : 15	**X_{15}13**
$C_{18}H_{37}Si(OEt)_3$ (**17**)	1 : 19	**X_{19}13**
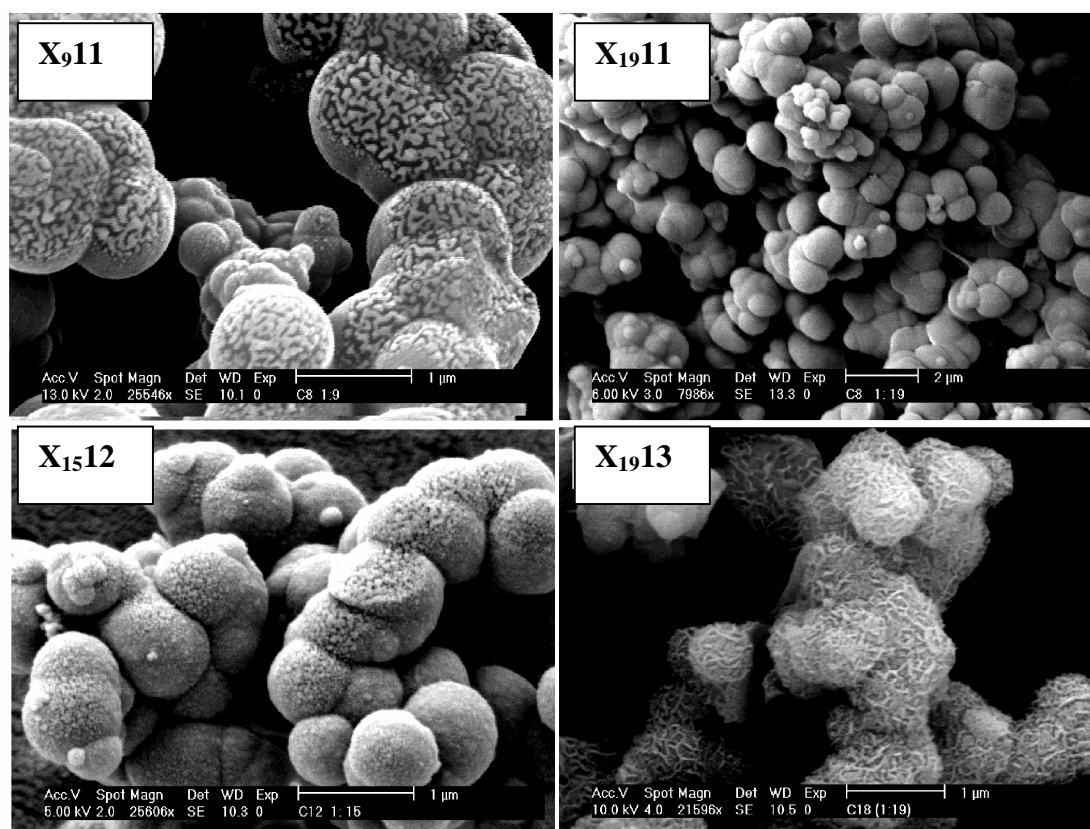
Figure 12. Scanning electron micrographs (SEM) of mesoporous stationary phases with different chain lengths.

The morphology of the xerogels was characterized by scanning electron microscopy (SEM). Figure 12 depicts the scanning electron micrographs of some xerogels (**$X_9$11**, **X_{19}11**, **X_{15}12**, **X_{19}13**). The xerogels form primary particles (diameter about 1 µm) which agglomerate to clusters with particle size distributions summarized in Table 10.

Table 10

Cluster particle size distribution of the materials

Xerogel	x_{10} [µm] [a]	x_{50} [µm] [b]	x_{90} [µm] [c]
$X_9$11	2.6	12.4	45.7
X_{15}11	3.3	12.9	30.6
X_{19}11	3.2	11.3	21.7
$X_9$12	2.7	7.9	23.4
X_{15}12	2.7	9.1	24.6
X_{19}12	2.3	7.2	32.8
$X_9$13	4.3	13.7	34.3
X_{15}13	4.3	9.8	20.0
X_{19}13	3.9	12.8	31.3

[a] 10% of the particles are smaller than the value indicated. [b] 50% of the particles are smaller than the value indicated. [c] 90% of the particles are smaller than the value indicated.

2.4.3. X-ray Diffraction and BET Measurements

The occurrence of peaks in the low angle powder X-ray diffraction (XRD) pattern proves unequivocal a high degree of organization of the xerogels. Some examples of XRD

profiles are depicted in Figure 13. All XRD patterns are similar and exhibit a broad diffraction peak corresponding to d_{100} spacing between 38 and 46 Å, respectively (Table 11). Higher order Bragg reflections are not observed. Measurements of the BET surface area and pore volume were performed determining N_2 adsoption-desorption isotherms for all materials (Table 11). All stationary phases show isotherms, which are typical of mesoporous structures.

In the case of the xerogels with C_{18} alkyl chains (**$X_9$13**, **X_{15}13**, **X_{19}13**) a certain amount of macroporosity could also be observed. For all polymers very large surface areas in the range of 960 to 1460 m^2/g were found. Stationary phases with a C_8 alkyl chain (**$X_9$11**, **X_{15}11**, **X_{19}11**) posses the highest BET areas with more than 1400 m^2/g. However, if longer alkyl chains are introduced into the xerogel, the surface areas decrease to ~1000 m^2/g. This fact clearly shows that the surface areas are peremptory of the amount of silica in the siloxane. The average pore diameters were determined from Horvath-Kawozoe pore size distribution curves [99]. The pore size of the ordered mesoporous material is between 13 and 19 Å. From these results a wall thickness of the stationary phase from 21 to 38 Å is derived. Thus it is possible to explicitly observe that the lowest wall thickness exists in the xerogels which are
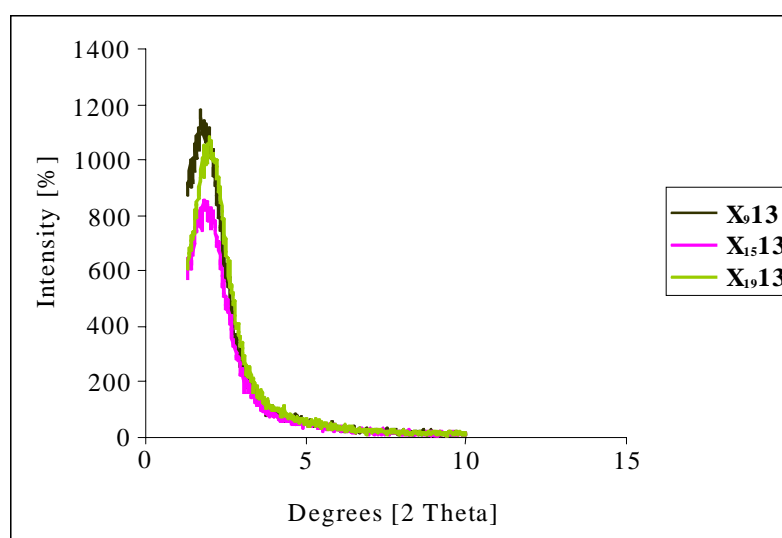
Figure 13. Powder X-ray diffraction patterns of **$X_9$13**, **X_{15}13**, and **X_{19}13**.

Table 11

XRD and BET dates of the stationary phases

Xerogel	S_{BET} [m^2/g]	Total pore volume [a] [cm^3/g]	HK pore size [Å]	XRD d_{100}-spacing [Å]	a_0 [b] [Å]	Wall thickness [c] [Å]
X$_9$11	1460	0.67	13	38	44	31
X$_{15}$11	1450	0.72	19	40	46	27
X$_{19}$11	1430	0.65	18	38	44	26
X$_9$12	1190	0.54	18	44	51	33
X$_{15}$12	1030	0.50	13	44	51	38
X$_{19}$12	960	0.51	13	42	49	36
X$_9$13	1000	1.27	19	46	53	34
X$_{15}$13	1060	1.09	19	46	53	34
X$_{19}$13	1080	0.88	19	44	51	32

[a] Determined by the t-plot method. [b] The repeat distance (a_0) between pores centers is calculated from the XRD data with the formula $a_0 = 2d_{100}/\sqrt{3}$. [c] The framework wall thickness is determined by subtracting the HK mesopore size from repeat distance between pore centers.

provided with an organotrialkoxysilane with a C_8 alkyl chain (**$X_9$11**, **X_{15}11**, **X_{19}11**).

2.4.4. Solid State NMR Spectroscopy

Solid-state NMR spectroscopy monitors the synthesis progress of the mesoporous materials and proves that the *n*-alkylsiloxanes with different chain lengths are bonded to a 3D network consisting of a polymer.

^{29}Si CP/MAS NMR investigations show an increasing intensity for the signals of T groups with an increasing amount of trialkoxyalkylsilane employed in the synthesis. Due to the loss of signals of T^1 structural elements in the spectra, it can be concluded that the crosslinking within these phases is very high. However, a quantification performed by peak deconvolution, does not show the expected values. Table 12 summarizes the educt

Table 12

Determination of T/Q-ratios by ^{29}Si CP/MAS NMR spectroscopy

Xerogel	Peak area data [ratio T/Q]
$X_9$1	1:5
X_{15}1	1:7
X_{19}1	1:10
$X_9$2	1:7
X_{15}2	1:11
X_{19}2	1:17
$X_9$3	1:13
X_{15}3	1:25
X_{19}3	1:28

ratios, whereas the values for the synthesized mesoporous polysiloxanes are given in Table 9. On the one hand, peak deconvolution proves a growing intensity of T^2 and T^3 signals at -56 and -65 ppm, respectively, with an increasing amount of trifunctional silane used
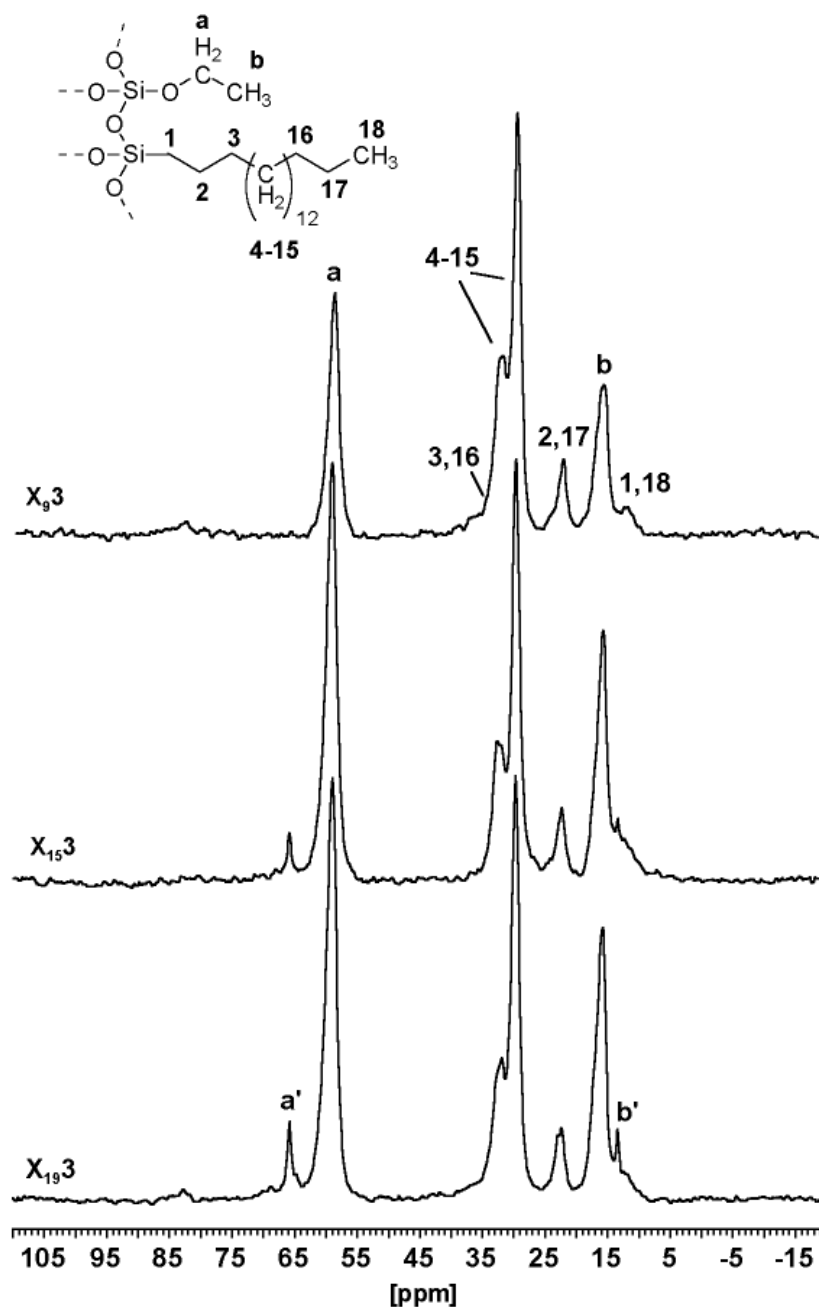
Figure 14. ^{13}C CP/MAS NMR spectra of $\mathbf{X_n13}$ (n = 9, 15, 19) mesoporous materials using different ratios trifunctional silane/TEOS. The $\mathbf{X_{15}13}$ and $\mathbf{X_{19}13}$ materials show the additional signals a' and b'.

in the synthesis procedure. The highest intensities for these silyl species are observed for **X$_n$11** materials, whereas only little signals of T groups are detected in the case of **X$_n$13** mesoporous phases. On the other hand, peak deconvolution indicates that silanes with C$_8$ chains lead to a higher trifunctional silane/TEOS ratio than expected, whereas C$_{18}$ chains obviously show a lower concentration in the sol-gel processed polysiloxanes. Trifunctional silane/TEOS ratios of 1:9, 1:15, 1:19 were applied in the syntheses. **X$_n$11** materials reveal values of 1:5, 1:7, and 1:10, respectively, whereas **X$_n$12** phases reveal values close to the educt ratios. **X$_n$13** mesoporous phases show only small amounts of polymerized alkyl silanes with ratios of 1:13, 1:25, and 1:28. This results may be explained by a better organization process due to a shorter chain length in the case of the octylsilanes and can be correlated with the elemental analysis. Obviously the chain length of the organosilane exerts a strong influence on the hydrophobic interactions between the alkyl chains of the silane and the template molecule.

^{13}C CP/MAS NMR spectra were also acquired for each of the new mesoporous stationary phase listed in Table 9. Representative spectra are shown in Figure 14 for the **X$_n$13** materials. The signals of the alkyl chain bonded to the polysiloxane backbone appear in the range from 12 to 35 ppm. In the case of the C$_{18}$ chains two different signals for the methylene groups at 30 and 32 ppm are observed. The signal at higher field is attributed to methylene groups with conformational disorder and a high level of mobility whereas the low field shifted signal confirms the presence of ordered, less mobile methylene groups in the alkyl chains of the mesoporous materials. The effect of different mobilities is only visible in the ^{13}C CP/MAS NMR spectra of the xerogels containing alkyl chains with 18 carbon atoms.

The intense signals at 60 (a) and 16 ppm (b) in the ^{13}C CP/MAS spectra depicted in Figure 13 are attributed to residual ethoxy groups of non-hydrolyzed TEOS. The relatively high portion of these groups is traced back to the templating pathway. The arrangement of TEOS during the condensation of the silica backbone does not allow a complete crosslinking

of the ortho silicate. The intensity of the signals at 66 (a') and 13 ppm (b') is dependent on the kind of material and increases in the sequence **X$_9$13** < **X$_{15}$13** < **X$_{19}$13** (Figure 13). **X$_n$11** (n = 9, 15, 19) xerogels do not show any of these additional signals in the ^{13}C CP/MAS NMR spectra, the **X$_n$12** (n = 9, 15, 19) materials reveal small signals only within the **X$_{19}$12** hybrid phases. It should be noted that the **X$_{19}$13** xerogel definitely shows the signals with the highest intensity which seems to be directly correlated to the intensity of the signals a and b of the ethoxy groups (Figure 14). An increasing signal intensity of ethoxy groups also leads to an increasing intensity of the additional signals a' and b'. Due to this fact and the chemical shift values of the signals a' and b', these additional resonances are attributed to another kind of ethoxy species. It is believed that these signals are caused by a crystalline substructure of the polymer backbone. Obviously, only longer alkyl chains encourage this arrangement. Measurements of the relaxation time of the protons in the rotating frame ($T_{1\rho H}$) support this thesis. Compared to the other signals in the ^{13}C CP/MAS NMR spectra, the $T_{1\rho H}$ relaxation times of the signals a and b are evidently longer pointing to a high mobility of the free ethoxy functions, which could be caused by fast rotational movement. Whereas the $T_{1\rho H}$ values of all other signals (including a' and b') are at about the same magnitude indicating a reduced mobility, which is typical for crystalline arrangements.

2.4.5. Analytical Electron Microcopy

Since organized silica are synthesized in a template synthesis using aliphatic amines, energy-dispersive X-ray analysis (EDX) has been performed to ensure the total removal of the template. Nitrogen could not be detected in any of the xerogels.

Energy filtering electron diffraction investigations were performed on phases of different alkyl modification covering the range from octyl (C$_8$) to octadecyl (C$_{18}$) chains using

zero-loss electrons at 120 keV beam energy. Figure 15 shows part of a series of diffraction patterns of the xerogel $X_{19}13$ with increasing electron dose. Due to the focused electron probe and the strong electron-matter interactions information can be obtained from specimen areas in the sub-micron range even from weakly scattering specimens composed of light elements.
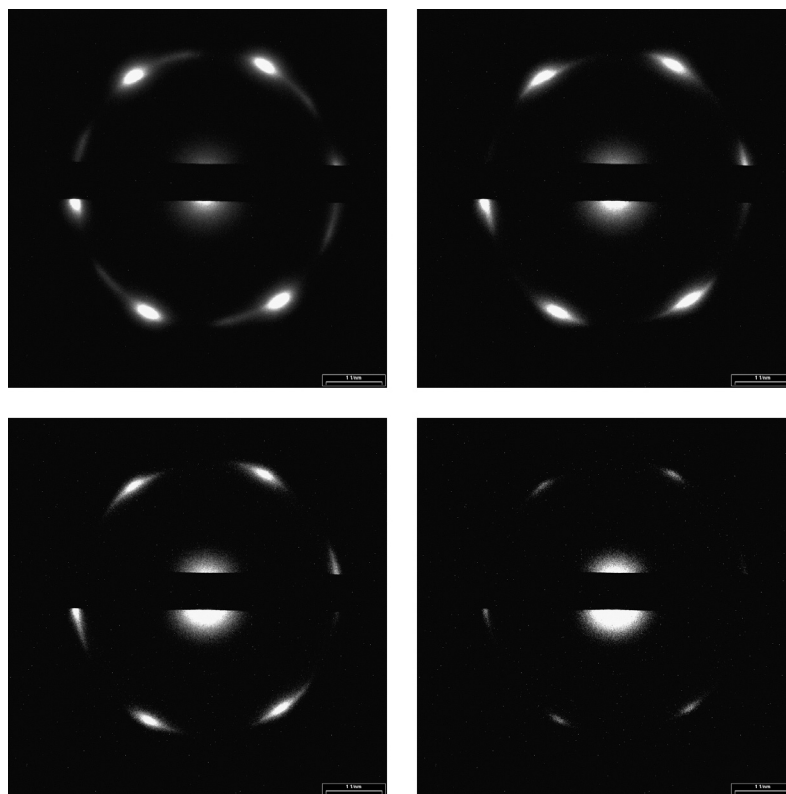
Figure 15. Electron diffraction pattern of ($X_{19}13$) with increasing electron dose (from top left to bottom right). The dose applied per image is $8 \cdot 10^{-4}$ C/cm^2 or 50 electrons/nm^2. The patterns were acquired with zero-loss electrons at 120 keV beam energy. The scale bars correspond to 1 nm^{-1}.

Single-crystalline diffraction patterns of hexagonal symmetry are recorded with silica $X_{9}11$, $X_{15}11$, $X_{15}13$, and $X_{19}13$. It has to be noted that the same pattern is reproducibly obtained from different sample grains, which are oriented randomly towards the electron beam. Lattice constants derived from these measurements are summarized in Table 13. A

pronounced broadening of Bragg reflections is observed and indicates strong disordering effects.

Table 13

Lattice constants of the alkyl substructure of compounds X_91, $X_{15}1$, $X_{15}3$, and $X_{19}3$ measured by electron diffraction. Critical doses that denote the charge per specimen area that has to be applied to reduce the reflection intensities to 10 % of their initial value are also summarized. In case of X_91 the reflections are too weak to derive a reliable critical dose

Compound	$X_{19}3$	X_91	$X_{15}1$	$X_{15}3$
Lattice constant [Å]	4.83 ($\pm$ 0.05)	5.16 ($\pm$ 0.13)	4.94 ($\pm$ 0.03)	4.79 ($\pm$ 0.06)
$d_{10\%}$ [10^{-3} C/cm^2]	5.02 ($\pm$ 0.09)	---	1.53 ($\pm$ 0.06)	4.41($\pm$ 0.06)

Organized silica ($X_{15}11$, $X_{15}13$, and $X_{19}13$) react very sensitive upon electron irradiation. This is a marked difference to the purely inorganic materials of Tanev and Pinnavaia [100]. This sensitivity is setting a limit to the obtainable information. Under these conditions, the lateral resolution of the microscope is not goverened by the optical quality of the instrument but by specimen destruction. In particular, assuming a necessary image contrast of 10 % and a signal-to-noise-ratio of 5, the Rose equation [104] predicts a lateral resolution of 30-50 Å with the doses reported below. Preparation techniques that may influence the solid-state structure were abandoned. Therefore, perfectly thin specimens are not encountered and direct imaging is not useful in the present investigations. However, as will be shown below, the electron beam induced specimen destruction can be readily used to prove that the alkyl substructure is giving rise to the electron diffraction patterns observed.
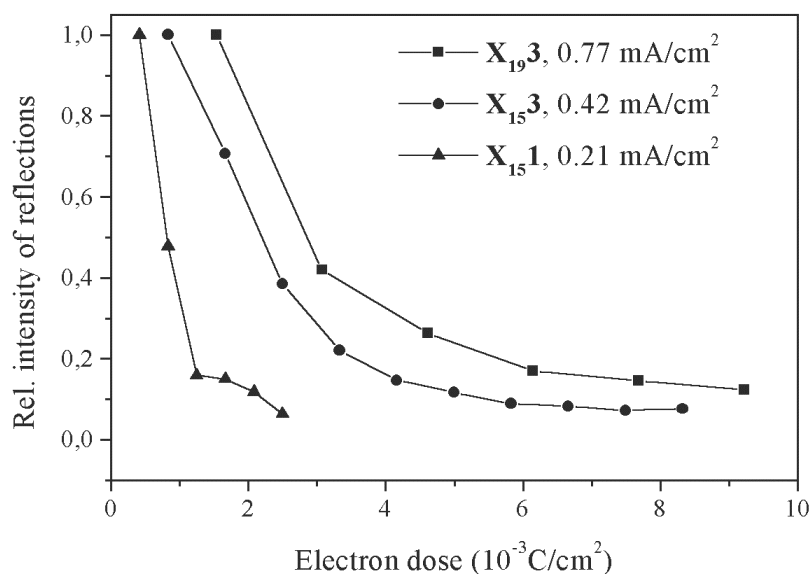
Figure 16. Decay of reflection intensity with increasing electron dose. Intensities have been normalized to the first value of each series but are not corrected for offset. The current density of each illumination series is indicated in the inlay. Critical doses of Table 13 are derived from these data.

Electron beam sensitivity was quantified in terms of decay of Bragg reflection intensity versus electron dose. This was accomplished by measuring the reflection intensity from exposure series recorded under constant current densities between 0.21-0.77 mA/cm^2. Under current densities as low as these damage of specimen is caused by ionization events and subsequent chemical reactions in the specimen, i.e. loss of hydrogen and crosslinking towards an amorphous carbonaceous matrix. Specimen heating can be clearly neglected [101-103,44] Intensities were normalized to the first value of each series. The result of this measurement is displayed in Figure 16. An exponential decay of reflection intensity with increasing electron dose was observed.

For the least sensitive compound **X$_{19}$13** an intensity loss of 90 % occurs within an electron dose of about d$_{10\%}$ = 0.005 C/cm^2 (300 electrons/nm^2). Octyl chains react even more sensitive, which indicates that the arrangement of alkyl chains is more easily perturbed in this case. This is in agreement with the larger selectivity of longer alkyl chains in the separation of aromatic hydrocarbons.

The diffraction patterns prove to be in agreement with those of the premelt ("rotator") phase of crystalline alkanes for several reasons [104]. (i) The hexagonal lattice constants of a = 4.79 – 5.16 Å are very similar to the value of 4.8 Å reported for the so called „rotator phase" of alkanes. (ii) The lattice constants of alkanes are nearly independent of the alkyl chain length. The lattice constants obtained for the compounds are summarized in Table 13 (**X$_9$11**, **X$_{15}$11**, **X$_{15}$13**, and **X$_{19}$13**)**.** They differ only by about 7 %. (iii) There is a pronounced broadening of reflections. This indicates the presence of strong disordering effects that can be ascribed to the conformal flexibility of alkyl chains. The same is observed with crystalline alkanes in the rotator phase. (iv) Monitoring the beam sensitivity in terms of reflection intensity versus electron dose renders critical doses in the order of $1\text{-}5\cdot10^{-3}$ C/cm^2 that are typical of alkanes [104]. Moreover, the intensity-dose profiles measured here equal those reported earlier as reported elsewhere [105].

Since silica generated by sol-gel processing are of amorphous character, it is concluded that in terms of electron diffraction the alkyl substituents form a single crystalline alkyl substructure within an amorphous silica matrix. It is noteworthy that the electron diffraction patterns do not depend on the orientation of the individual sample grains. Therefore, the alkyl chains exhibit the same cross sectional view towards the electron beam, regardless of the orientation of the individual sample grain, and the alkyl substructure forms symmetric enclosures in the silica matrix, i.e. micellae rather than tubular arrangements. This matches the results obtained with mesoporous materials synthesized in a similar procedure [6, 100].

2.4.6. Chromatography

The chromatographic performance of each stationary phase was investigated with
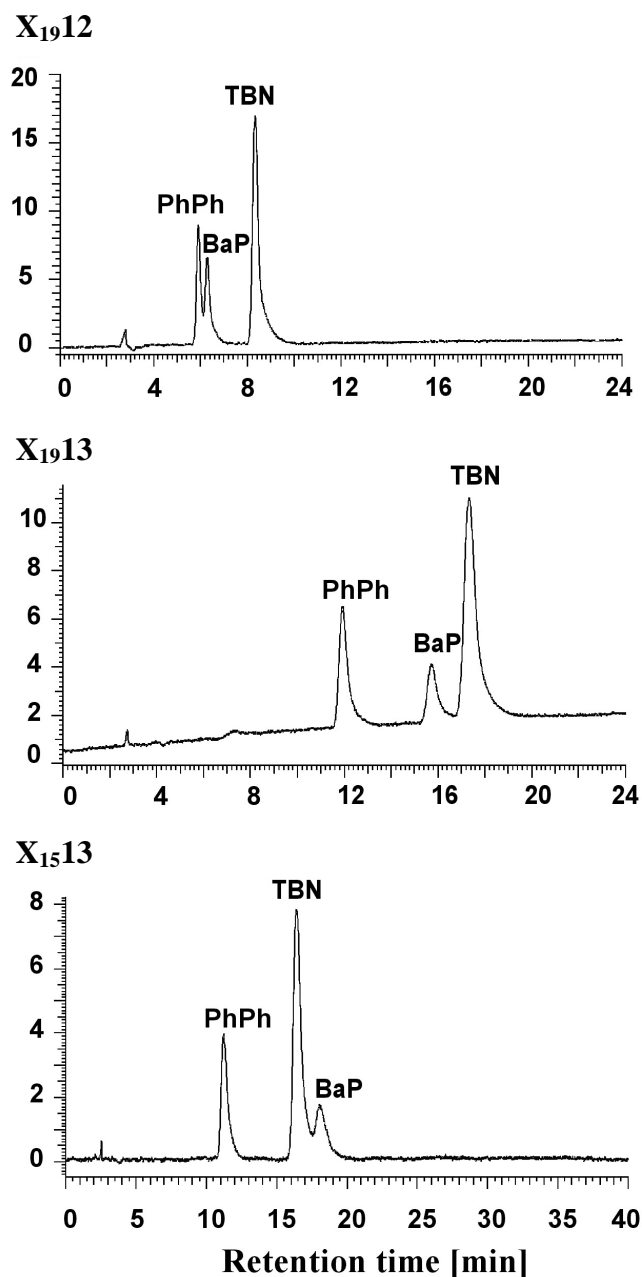
Figure 17. Separation of three polycyclic aromatic hydrocarbons (SRM869): PhPh (phenanthro[3-4,*c*]phenanthrene), BaP (benzo[*a*]pyrene), TBN (1,2:3,4:5,6:7,8-tetrabenzo-naphthalene). As stationary phases the ordered materials $X_{19}12$, $X_{19}13$, and $X_{15}13$ are used.

SRM 869a [106], a shape selectivity test mixture consisting of 1,2-3,4-5,6-7,8-tetrabenzonaphthalene (TBN), phenanthro[3,4-c]phenanthrene (PhPh), and benzo[a]pyrene (BaP) in acetonitrile. Depending on the elution order of the three components, column selectivity can be predicted for complex polyaromatic hydrocarbon (PAH) mixtures and even helps to characterize the column selectivity for other classes of compounds such as carotene isomers. In recent studies, SRM 869a has also been used to characterize column selectivity for different alkyl chain length stationary phases. In general, late elution of benzo[a]pyrene (BaP) relative to 1,2-3,4-5,6-7,8-tetrabenzonaphthalene (TBN) indicates an increasing shape selectivity. Figure 17 depicts the HPLC runs employing the xerogles $\mathbf{X_{19}12}$, $\mathbf{X_{15}13}$, and $\mathbf{X_{19}13}$ as stationary phases. The elution order BaP < TBN in the case of the $\mathbf{X_{19}12}$ phases indicates a poor shape selectivity and therefore a reduced recognition towards geometric isomers. An increasing chain length directly leads to a higher retention time of BaP and conclusively to higher shape selectivity of the $\mathbf{X_n13}$ (n = 9, 15, 19) stationary phases. However, the xerogel $\mathbf{X_{15}13}$ shows the elution order TBN < BAP which indicates a good selectivity for geometric isomers.

Separations of a mixture of 16 priority pollutant PAH´s (SRM 1647c [107]) were employed for further characterization of the properties of the mesoporous stationary phases. Only phases with a very high shape selectivity are able to resolve all 16 priority pollutants. Figure 18 shows the chromatographic runs using the xerogels $\mathbf{X_{19}12}$, $\mathbf{X_{15}13}$, and $\mathbf{X_{19}13}$ as stationary phases; peak assignment is also indicated. $\mathbf{X_{19}12}$ indicates a low shape selectivity due the elution order indeno[1,2,3-cd]pyrene (16) < benzo[ghi]perylene (15), whereas the $\mathbf{X_{19}13}$ material obviously leads to better selectivity. In comparison to the shorter C_{12} chains, the C_{18} chains posses improved recognition towards geometric isomers which directly results in better separations. The compounds benzo[a]anthracene (9), chrysene (10), and benzo[b]fluoranthene (11), benzo[k]fluoranthene (12) show much better separation behavior
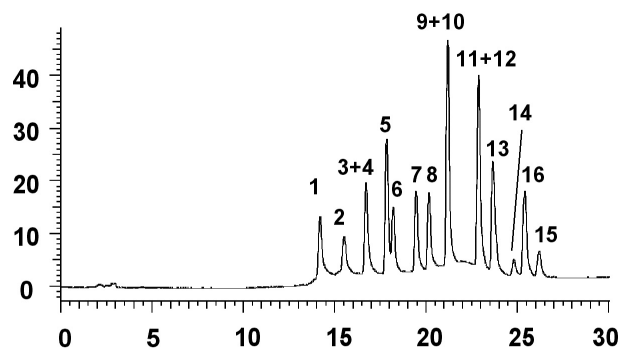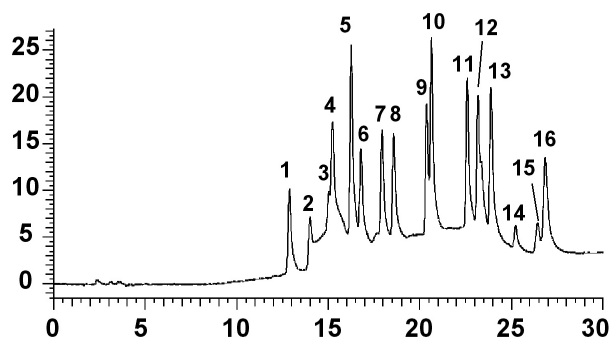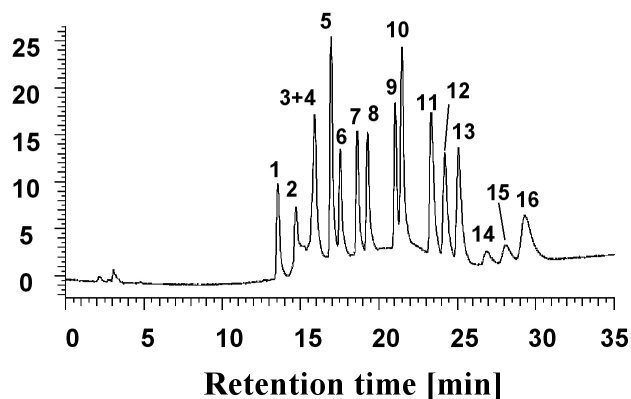
Figure 18. Separation of the 16 priority pollutant polycyclic aromatic hydrocarbons (SRM1647c: 1 naphthalene, 2 acenaphthylene, 3 acenaphthene, 4 fluorene, 5 phenanthrene, 6 anthracene, 7 fluoranthene, 8 pyrene, 9 benzo[*a*]anthracene, 10 chrysene, 11 benzo[*b*]fluoranthene, 12 benzo[*k*]fluoranthene, 13 benzo[*a*]pyrene, 14 dibenz[*a,h*]anthracene, 15 benzo[*ghi*]perylene, 16 indeno[1,2,3-*cd*]pyrene) on the mesoporous stationary phases $X_{19}12$, $X_{19}13$, $X_{15}13$.

than in the case of the xerogels with shorter chain lengths. A strong hint for better selectivity gives the elution order of the compounds benzo[*ghi*]perylene (15) and indeno[1,2,3-*cd*]pyrene (16). With C_{12} stationary phases [X_n12 (n = 9, 15, 18)], the order of elution shows exactly this behavior, whereas the increase of the chain length up to 18 carbon atoms [X_n13 (n = 9, 15, 18)] leads to an exchange in elution order, and benzo[*ghi*]perylene (15) elutes in front of indeno[1,2,3-*cd*]pyrene (16). However, the best separations of the 16 PAH´s was achieved by using the xerogel $X_{15}13$ as stationary phase. Only the compounds acenaphthene (3) and fluorene (4) are not separated which proofs the results of the test mixture SRM 869a and indicates a high shape selectivity of this material.

A big advantage of these novel stationary phases is the fast synthesis procedure and the wide variety of functional groups that can be easily bound to the matrix. The separations in Figure 6 and 7 proof that the xerogels can be used as stationary phases in HPLC with high selectivity. Although possessing a very high pore volume, the mesoporous materials are pressure stable and are applicable in a wide range.

2.4.7. Conclusion

With the direct synthesis of new inorganic-organic hybrid materials in the presence of a surfactant and their first application in HPLC was a consequent step in the further development of RP materials. For the reproducible access to the novel mesoporous, nanostructured stationary phases X_911-$X_{19}13$ a simple one step process has been established. A suitable pathway is the sol-gel processing of *n*-alkyl substituted trialkoxysilanes with tetraethoxysilane (TEOS) as crosslinker and an aliphatic amine as template molecule. It was demonstrated that the new materials show a similar separation performance like analogous surface modified silicas (RP C_{18} phases), although the particle size is smaller compared to

conventional stationary phases, which were successfully employed in HPLC. For the first time a local crystalline substructure of alkyl chains within a silica polymer was found by electron diffraction. A necessary precondition for the detection of a local crystalline substructure with EFTEM is the *trans*-alignment of an essential part of the alkyl chains. Additional signals in the ^{13}C CP/MAS NMR spectra of the materials are interpreted in this way and support this hypothesis. The understanding of the arrangement of the recognition centers is of essential importance in the design of novel stationary phases for HPLC. Recent investigations on C_{30} alkyl surface modified silicas confirm an increase of shape selectivity with increasing portions of *trans* aligned alkyl chains in the stationary phase.

For the solution of other ambitions separation problems a modification of the alkyl chains with functionalized groups comes into question. Furthermore it is possible to control the pore size of the stationary phases by the utilization of other template molecules (e.g. block polymers) for different requirements in HPLC. In such a case C_{30} alkyl chains can be co-condensed with TEOS, to separate larger natural substances, like carotinoids.

3.   EXPERIMENTAL SECTION

3. 1.   General Remarks

All reactions and manipulations were carried out under argon with the usual Schlenck techniques. Ethanol was dried with sodium and phthalic acid diethyl ester and distilled. All other solvents were distilled from sodium benzophenone or calcium hydride. H_2O was distilled under inert gas prior to use. All solvents and reagents were stored under argon.

3.1.1.   Reagents

$[\mu\text{-ClRh(CO)}_2]_2$ and $[\mu\text{-ClIr(COE)}_2]_2$ were purchased from Aldrich. All other chemicals were bought from Fluka or Merck (Germany). The co-condensation agents **4(D^0)**, **4(T^0)**, **5(D^0)**, and **5(T^0)** were synthesized according to literature.

3.1.2.   Elemental Analyses, IR, Particle Size Distribution and Mass Investigations

Elemental analyses were carried out on a Vario EL (Elementar Analytische Systeme Hanau). IR data were obtained on a Bruker IFS 48 FT–IR spectrometer. Mass spectra (FD) were acquired on a Finnigan MAT 711A instrument (8 kV, 333 K), EI–spectra were recorded on a TSQ Finnigan (70 eV, 473 K) and reported as mass/charge (*m/z*). Particle size distributions were determined by laser diffraction on a Sympatec Helos instrument in ethanolic suspension.

3.1.3. NMR Spectroscopy in Solution

Solution nuclear magnetic resonance spectra were recorded on a Bruker DRX 250 spectrometer (field strength 5.87 T) at 296 K. Frequencies are as follows: ^{1}H NMR: 250.13 MHz, ^{31}P{^{1}H} NMR: 101.25 MHz (referenced to 85 % H_3PO_4), ^{13}C{^{1}H} NMR: 62.90 MHz, ^{29}Si{^{1}H} NMR: 49.69 MHz. Chemical shifts in the ^{1}H and ^{13}C{^{1}H} NMR spectra were measured relative to partially deuterated solvent peaks which are reported relative to TMS.

3.1.4. Solid State NMR Measurements

CP/MAS solid state NMR spectra were recorded on Bruker DSX 200 and Bruker ASX 300 (temperature dependent measurements) multinuclear spectrometers equipped with wide bore magnets (field strength 4.7 T and 7.05 T). Magic angle spinning was applied up to 10 kHz (4 mm ZrO_2 rotors) and 3 – 4 kHz (7 mm ZrO_2 rotors), respectively. Frequencies and standards: ^{31}P, 81.961 MHz (4.7 T), 121.442 MHz (7.05 T) [85% H_3PO_4, $NH_4H_2PO_4$ ($\delta = 0.8$) as second standard]; ^{13}C, 50.228 MHz (4.7 T), 75.432 MHz (7.05 T), [TMS, carbonyl resonance of glycine ($\delta = 176.05$) as second standard]; ^{29}Si, 39.73 MHz (4.7 T), 59.595 MHz (7.05 T), (Q_8M_8 as second standard). All samples were packed under exclusion of molecular oxygen. The cross polarization constants T_{XH} were determined by variation of the contact time T_c (14 – 16 experiments). The proton relaxation times in the rotating frame $T_{1\rho H}$ were measured by direct proton spin lock–τ–CP experiments [55]. The relaxation parameters were obtained using Bruker software SIMFIT. Peak deconvolution of the spectra were performed with the Bruker softwear WINFIT using Voigtian line shapes. For the quantification of the silyl species in the polysiloxanes, ^{29}Si CP/MAS NMR contact time variations experiments were carried out and the obtained quasi 2D–data set was analyzed with XWINNMR. The

relative amounts I_0 of each of the D^i and T^n species in one sample were calculated by inserting their peak areas of the deconvoluted spectra $I(T_c)$, the individual T_{SiH} data, and the common $T_{1\rho H}$ value into the following equitation [53].

$$I(T_c) = \frac{I_0}{(1 - T_{SiH}/T_{1\rho H})}(e^{-T_c/T_{1\rho H}} - e^{-T_c/T_{SiH}}) \qquad (1)$$

If the boundary condition $T_{SiH} \ll T_{1\rho H}$ [54] could not be considered, the quantification of the silyl species was performed by deconvolution of the ^{29}Si CP/MAS spectra ($T_c = 5$ ms) [39] or by a ^{29}Si HPDEC/MAS NMR experiment [recycle delay 20 s, pulse length 3.5 μs (~ 45°)] followed by peak deconvolution.

3.1.5. EXAFS Measurements

The EXAFS measurements were performed at the Ir-L_3-edge at 11215 eV at the beamline X1.1 at the Hamburger Synchrotronstrahlungslabor (HASYLAB) at DESY, Hamburg at 20 °C, with a Si(111) double crystal monochromator under ambient conditions (5.46 GeV, beam current 120 mA). Data were collected in transmission mode with ion chambers. Energy calibration was monitored with 20 μm thick platin metal foil at L_3-edge at 11564 eV. All measurements were performed under an inert gas atmosphere. The samples were prepared of a mixture of **X7** and polyethylene. Data were analyzed with a program package specially developed for the requirements of amorphous samples [108]. The program AUTOBK of the University of Washington [109] was used for background removal, and the program EXCURV92 [110] was used for the evaluation of the XAFS function. The resulting EXAFS function was weighted with k^3. Data analysis in k space was performed according to

the curved-wave multiple-scattering formalism of the program EXCURV92. The mean free path of the scattered electrons was calculated from the imaginary part of the potential (VPI was set to – 4.00), the amplitude reduction factor AFAC was fixed at 0.8, and an overall energy shift ΔE_0 was introduced to fit the data. In the fitting procedure the intermolecular coordination numbers were varied and the intramolecular coordination numbers were fixed according to the known values of the ligands around the iridium atom of **X7**.

3.1.6. SEM and EDX Investigations

Scanning electron microscopy [111] was performed on a XL 30 scanning electron microscope by *Philips* equipped with an DX-4 energy dispersive X-ray detection system by *EDAX*. This consists of a liquid nitrogen cooled lithium-drifted silicon detector with an active area of 10 mm^2 and the eDXi 2.11 software package. The detector resolution is 149 eV at MnK_α (5.984 keV) and the sample-detector distance is 50 mm in the present system. The sample powder was placed on a commercial specimen stub covered with an adhesive tab and subsequently provided with a sputtered 20 nm gold layer to ensure conductivity. The primary beam energy was 20 keV during all investigations. A probe current of 192 pA was applied for recording electron micrographs, whereas X-ray emission spectra were acquired under spot illumination applying a probe current of 569 pA for 400 live seconds (dead time approx. 33%). Measurements were repeated several times at various specimen positions to ensure reproducibility. Quantification of X-ray spectra was carried out employing the ZAF correction procedure [112-114] after subtraction of the Bremsstrahlung background.

3.1.7. Energy Filtering Transmission Electron Microscope (EFTEM)

Electron diffraction studies were carried out on a LEO EM 912 Ω energy filtering transmission electron microscope (EFTEM) equipped with Köhler illumination, micro-dose focussing system, and a cooled high speed slow scan CCD (charge coupled device) camera. All diffraction patterns displayed here were obtained using zero-loss filtered electrons at 120 keV with an untilted specimen stage and were calibrated by comparison to a polycrystalline gold standard at the same camera length. The temperature inside the specimen area of the microscope was approximately 30°C. As the silica spheres are by far too thick for transmission electron microscopic investigations, the sample powder was thoroughly grounded in a mortar, suspended in ethanol and treated in an ultrasonic bath for 10 min. The sample was transferred to commercial 400 mesh coppers grids covered with an amorphous perforated 10 nm carbon foil as specimen support.

3.1.8. Catalysis

The hydroformylation experiments were carried out in a 100 ml stainless steel autoclave equipped with a mechanical stirring bar. The autoclave was flushed with argon prior to the introduction of the reaction mixture (5 µmol of catalyst with respect to rhodium, 80 mmol of 1-hexene, and 30 ml of the solvent). The reaction mixture was set under CO pressure and stirred for 30 min prior to hydrogen introduction. After stirring for 5 min the mixture was heated to the required temperature. The quantitative analyses were performed on a GC 6000 Vega Series 2 (Carlo Erba Instruments) with an FID and a capillary column CP Sil 88 [17 m, carrier gas helium (50 kPa); integrator Hewlett Packard 3390 A]. Leaching

investigations were carried out with a Varian Spectr AA 20 Plus atomic absorption spectrometer.

3. 2.   Preparation of the Compounds

3.2.1.   Synthesis of the Monomers

3.2.1.1.   *N-[p-(Diphenylphosphinyl)phenyl]-N´-[(triethoxysilyl)propyl]urea [2(T⁰)]*

To a solution of **1** (12.6 g, 45.4 mmol) in 30 ml of dichloromethane a solution of triethoxysilylpropylisocyanate (11.2 g, 45.4 mmol) in 10 ml of dichloromethane was slowly added. After stirring overnight the solvent was reduced in vacuum and **2(T⁰)** was obtained as a colorless waxy solid which is sensitive to moisture and air. Yield: 21.3 g (89.4 %). ^{1}H NMR (CDCl$_3$): δ = 7.69 - 7.05 (m, 14H, H-phenyl), 3.67 (q, $^3J_{HH}$ = 6.91 Hz, 6H, O–CH_2–CH$_3$), 3.08 (m, 2H, NH–CH_2–CH$_2$), 1.51 (m, 2H, CH$_2$–CH_2–CH$_2$), 1.11 (t, $^3J_{HH}$ = 6.91 Hz, 9H, O–CH$_2$–CH_3), 0.52 (m. 2H, CH$_2$–CH_2–Si). ^{13}C{^{1}H} NMR (CDCl$_3$): δ = 156.1 (s, NH–CO–NH), 140.6 – 119.2 (m, C–phenyl), 58.5 (s, O–CH$_2$–CH$_3$), 42.7 (s, NH–CH$_2$–CH$_2$), 23.7 (CH$_2$–CH$_2$–CH$_2$), 18.4 (s, O–CH$_2$–CH$_3$), 7.8 (s, CH$_2$–CH$_2$–Si). ^{31}P{^{1}H} NMR (CDCl$_3$): δ = – 5.5. ^{29}Si{^{1}H}–NMR (C$_6$D$_6$): δ = – 45.1. IR (KBr, cm^{-1}): 3311 [ν(NH)], 1643 [ν(C≡O)]. MS (FD); *m/z*: 524 [M$^+$]. Anal. Found: C, 64.71; H, 6.90; N, 5.07. Calc. for C$_{28}$H$_{37}$N$_2$O$_4$PSi: C, 64.10; H, 7.11; N, 5.34%.

3.2.1.2. Chlorocarbonyl-bis{N-[p-(diphenylphosphinyl)phenyl]-N´-[(triethoxysilyl)propyl] urea}rhodium(I) [3(T⁰)]

To a solution of [µ-ClRh(CO)$_2$]$_2$ (0.24 g, 0.62 mmol) in 10 ml of benzene a solution of **2(T^0)** (1.31 g, 2.49 mmol) in 10 ml of benzene was added dropwise. The reaction mixture was stirred for 1h at ambient temperature. The solvent was removed in vacuum and the residual waxy solid was dissolved in 10 ml of *n*-hexane. After stirring for 30 min the solvent was removed under reduced pressure and **3(T^0)** was obtained as a yellow microcristalline solid which is sensitive to moisture and air. Yield: 1.49 g (98.4 %). ^{1}H NMR (CD$_2$Cl$_2$): δ = 7.97 – 7.28 (m, 14H, H–phenyl), 3.71 (q, $^3J_{HH}$ = 7.22 Hz, 6H, O–CH_2–CH$_3$), 3.03 (m, 2H, NH–CH_2– CH$_2$), 1.48 (m, 2H, CH$_2$–CH_2–CH$_2$), 1.11 (t, $^3J_{HH}$ = 7.22 Hz, 9H, O–CH$_2$–CH_3), 0.52 (m. 2H, CH$_2$–CH_2–Si). ^{13}C{^{1}H} NMR (CD$_2$Cl$_2$): δ = 156.0 (s, NH–CO–NH), 143.0 – 118.1 (m, C– phenyl), 58.8 (s, O–CH$_2$–CH$_3$), 43.0 (s, NH–CH$_2$–CH$_2$), 24.1 (CH$_2$–CH$_2$–CH$_2$), 18.6 (s, O– CH$_2$–CH$_3$), 8.0 (s, CH$_2$–CH$_2$–Si). ^{31}P{^{1}H} NMR (CD$_2$Cl$_2$): δ = 29.2 (d, $^1J_{RhP}$ = 124.7 Hz). IR (KBr, cm^{-1}): 3331 [ν(NH)], 1980 [ν(Rh–C≡O)], 1693 [ν(NH–C=O–NH)]. MS (EI); *m/z*: 1214 [M$^+$], 1186 [M$^+$ – CO]. Anal. Found: C, 55.79; H, 5.96; N, 4.28. Calc. for C$_{57}$H$_{74}$ClN$_4$O$_9$P$_2$RhSi$_2$: C, 56.31; H, 6.14; N, 4.61%.

3.2.1.3. p-Bromo[4-(trichlorosilyl)butyl]benzene (7)

A mixture of *p*-bromobutenylbenzene (**6**) (27.6 g, 130.7 mmol), trichlorosilane (26.6 g, 196.1 mmol) and hexachloroplatinic(IV) acid (15 mg, 0.029 mmol) in 25 ml of THF was stirred 1 d at room temperature. Distillation under vacuum affords **7** as a colorless, airstable oil which is sensitive to moisture. Yield 33.1 g (73.1%), b. p. 145°C (0.3 mbar). ^{1}H NMR (CDCl$_3$): δ = 7.31 (d, $^3J_{HH}$ = 8.16 Hz, 2H, 2,6-benzene), 6.96 (d, $^3J_{HH}$ = 8.16 Hz, 2H, 3,5-

benzene), 2.51 (t, $^3J_{HH}$ = 6.91 Hz, 2H, Br–C$_6$H$_4$–CH_2), 1.56 (m, 4H, CH$_2$–CH_2–CH_2–CH$_2$), 1.34 (m, 2H, CH_2–SiCl$_3$). ^{13}C{^{1}H} NMR (CDCl$_3$): δ = 141.1 (s, C–CH$_2$), 131.8 (s, CH–CBr), 130.5 (s, CH–C–CH$_2$), 120.0 (s, CBr), 35.1 (s, C$_6$H$_4$–CH$_2$), 33.8 (s, C$_6$H$_4$–CH$_2$–CH$_2$), 24.5 (s, CH$_2$–CH$_2$–SiCl$_3$), 22.3 (s, CH$_2$–SiCl$_3$).

3.2.1.4. *p-Bromo[4-(triisopropoxysilyl)butenyl]benzene [8(T^0)]*

Under ambient temperature triisopropyl orthoformate (67.4 g, 354.0 mmol) was added dropwise to *p*-bromo[4-(trichlorosilyl)butyl]benzene (**7**) (33.1 g, 95.5 mmol). After the addition the solution was stirred for 3 d. Distillation under vacuum affords **8(T^0)** as a colorless, airstable oil which is sensitive to moisture. Yield 36.4 g (91.3%), b. p. 135°C (0.1 mbar). ^{1}H NMR (CDCl$_3$): δ = 7.28 (d, $^3J_{HH}$ = 8.17 Hz, 2H, 2,6-benzene), 6.95 (d, $^3J_{HH}$ = 8.16 Hz, 2H, 3,5-benzene), 4.10 (hept, $^3J_{HH}$ = 6.28 Hz, 3H, O–CH), 2.46 (t, $^3J_{HH}$ = 7.85 Hz, 2H, Br–C$_6$H$_4$–CH_2), 1.54 (m, 2H, C$_6$H$_4$–CH$_2$–CH_2), 1.38 (m, 2H, CH_2–CH$_2$–Si(OiPr)$_3$), 1.09 (d, $^3J_{HH}$ = 6.28 Hz, 18H CH$_3$), 0.52 (m, 2H, CH$_2$–Si(OiPr)$_3$). ^{13}C{^{1}H} NMR (CDCl$_3$): δ = 142.1 (s, C–CH$_2$), 131.6 (s, CH–CBr), 130.6 (s, CH–C–CH$_2$), 119.6 (s, CBr), 65.2 (s, CH–O), 35.3 (s, C$_6$H$_4$–CH$_2$), 35.1 (s, C$_6$H$_4$–CH$_2$–CH$_2$), 25.7 (d, $^3J_{HH}$ = 6.29 Hz, 18H, CH$_3$), 23.0 (s, CH$_2$–CH$_2$–Si(OiPr)$_3$), 12.2 (s, CH$_2$–Si(OiPr)$_3$). ^{29}Si{^{1}H} NMR (CDCl$_3$): δ = –48.8 (s). MS (EI); *m/z*: 418 [M$^+$]. Anal. Calc. (C$_{19}$H$_{33}$BrO$_3$Si): C 54.67; H 7.97. Found: C 54.61; H 7.90.

3.2.1.5. *[p-Butyl(4-triiosopropoxysilyl)phenyl]diphenylphosphine [9(T^0)]*

Magnesium (1.20 g, 50.0 mmol) and 50 ml of THF were placed in a three-necked flask equipped with a magnetic stirrer, a condenser, and a dropping funnel. After activation of the

magnesium by some pieces of iodine, a solution of **8(T^0)** (20.87 g, 50.0 mmol) in 50 ml of THF was added dropwise. The reaction mixture was refluxed for 3 h, decanted from excess magnesium and cooled to –20°C. Subsequently dichlorophenylphosphine (10.14 g, 45.0 mmol) was added to the Grignard solution. The mixture was stirred for 12 h at room temperature. THF was removed and *n*-pentane (300 ml) was added. After filtration and removal of the solvent under vacuum, an oily product was obtained which is sensitive to moisture and air. Yield 17.5 g (63.0%). ^{1}H NMR (CDCl$_3$): δ = 7.24 – 7.08 (m, 14H, phenyl + phenylene), 4.10 (hept, $^3J_{HH}$ = 6.27 Hz, 3H, O–CH), 2.53 (t, $^3J_{HH}$ = 7.85 Hz, 2H, C$_6$H$_4$–CH_2), 1.58 (m, 2H, C$_6$H$_4$–CH$_2$–CH_2), 1.37 (m, 2H, CH_2–CH$_2$–Si(OiPr)$_3$), 1.09 (d, $^3J_{HH}$ = 6.28 Hz, 18H, CH$_3$), 0.54 (m, 2H, CH$_2$–Si(OiPr)$_3$). ^{13}C{^{1}H} NMR (CDCl$_3$): δ = 143.7 (s, *para*-C-phenylene), 137.5 (d, $^1J_{PC}$ = 10.6 Hz, *ipso*-C-phenyl), 133.8 (d, ^2J(PC) = 20.2 Hz, *ortho*-C-phenylene), 133.7 (m, *ipso*-phenylene), 133.5 (d, $^2J_{PC}$ = 19.1 Hz, *ortho*-C-phenyl), 128.7 (d, $^3J_{PC}$ = 7.4 Hz, *meta*-C-phenylene), 128.5 (d, $^1J_{PC}$ = 9.4 Hz, *ipso*-C-phenylene), 128.3 (d, $^3J_{PC}$ = 6.7 Hz, *ortho*-C-phenyl), 64.8 (s, CH–O), 35.3 (s, C$_6$H$_4$–CH$_2$), 34.7 (s, C$_6$H$_4$–CH$_2$–CH$_2$), 25.5 (CH$_3$), 22.6 (s, CH_2–CH$_2$–Si(OiPr)$_3$), 11.8 (s, CH$_2$–Si(OiPr)$_3$). ^{29}Si{^{1}H} NMR (CDCl$_3$): δ = –48.6 (s). ^{31}P{^{1}H} NMR (CDCl$_3$): δ = –4.98 (s). MS (EI); *m/z*: 522 [M$^+$]. Anal. Calc. (C$_{31}$H$_{43}$O$_3$PSi): C 71.23; H 8.29. Found: C 70.61; H 8.23.

3.2.1.6. [p-Butyl(4-trimethoxysilyl)phenyl]diphenylphosphine [10(T^0)]

A solution of **9(T^0)** (5.0 g, 9.6 mmol) in methanol (20 ml) was stirred at ambient temperature for 24 h in the presence of *p*-toluenesulfonic acid (10 mg, 0.05 mmol). Then the solvent was removed under vacuum. The residue was dissolved in methanol (20 ml) and the mixture was stirred for a further day. To achieve a complete exchange reaction, this operation was repeated three times. A bright yellow oily product was obtained which is sensitive to

moisture and air. Yield 3.5 g (83%). ^{1}H NMR (CDCl$_3$): δ = 7.26 – 7.07 (m, 14H, phenyl +

phenylene), 3.49 (s, 9H, O–CH$_3$), 2.55 (t, $^3J_{HH}$ = 7.85 Hz, 2H, C$_6$H$_4$–CH$_2$), 1.60 (m, 2H,

C$_6$H$_4$–CH$_2$–CH$_2$), 1.43 (m, 2H, CH$_2$–CH$_2$–Si(OMe)$_3$), 0.62 (m, 2H, CH$_2$–Si(OMe)$_3$). ^{13}C{^{1}H}

NMR (CDCl$_3$): δ = 143.5 (s, *para*-C-phenylene), 137.5 (d, $^1J_{PC}$ = 10.3 Hz, *ipso*-C-phenyl),

133.9 (d, $^2J_{PC}$ = 20.2 Hz, *ortho*-C-phenylene), 133.6 (d, $^1J_{PC}$ = 9.2 Hz, *ipso*-C-phenylene),

133.5 (d, $^2J_{PC}$ = 19.3 Hz, *ortho*-C-phenyl), 128.7 (d, $^3J_{PC}$ = 7.4 Hz, *meta*-C-phenylene), 128.6

(s, *para*-C-phenyl), 128.5 (d, $^3J_{PC}$ = 6.7 Hz, *ortho*-C-phenyl), 50.5 (s, O–CH$_3$), 35.4 (s, C$_6$H$_4$–

CH$_2$), 34.6 (s, C$_6$H$_4$–CH$_2$–CH$_2$), 22.3 (s, CH$_2$–CH$_2$–Si(OMe)$_3$), 9.0 (s, CH$_2$–Si(OMe)$_3$).

^{29}Si{^{1}H} NMR (CDCl$_3$): δ = –41.3 (s). ^{31}P{^{1}H} NMR (CDCl$_3$): δ = –5.02 (s). MS (EI); *m/z*:

438 [M$^+$]. Anal. Calc. (C$_{25}$H$_{31}$O$_3$PSi): C 68.47; H 7.12. Found: C 68.67; H 7.14.

3.2.1.7. *Carbonylchlorobis[diphenyl[4-[4-(trimethoxysilyl)butyl]phenyl]phosphane-κP]rhodium(I) [11(T^0)]*

To a solution of [μ-ClRh(CO)$_2$]$_2$ (0.25 g, 0.64 mmol) in 10 ml of benzene was added

dropwise a solution of **10(T^0)** (1.12 g, 2.57 mmol) in 10 ml of benzene. The reaction mixture

was stirred for 1 h at ambient temperature. After drying the product for 3 h in vacuum a

yellow waxy solid was obtained which is sensitive to moisture and air. Yield: 1.26 g, (94.5%).

^{1}H NMR (CD$_2$Cl$_2$): δ = 7.61 – 7.18 (m, 14H, phenyl + phenylene), 3.47 (s, 9H, O–CH$_3$), 2.60

(t, $^3J_{HH}$ = 7.85 Hz, 2H, C$_6$H$_4$–CH$_2$), 1.59 (m, 2H, C$_6$H$_4$–CH$_2$–CH$_2$), 1.40 (m, 2H, CH$_2$–CH$_2$–

Si(OMe)$_3$), 0.61 (m, 2H, CH$_2$–Si(OMe)$_3$). ^{13}C{^{1}H} NMR (CD$_2$Cl$_2$): δ = 144.7 (s, *para*-C-

phenylene), 137.5, 133.8, 132.6, 129.3, 127.4 (m, phenyl + phenylene), 49.5 (s, O–CH$_3$), 34.6

(s, C$_6$H$_4$–CH$_2$), 33.7 (s, C$_6$H$_4$–CH$_2$–CH$_2$), 21.6 (s, CH$_2$–CH$_2$–Si(OMe)$_3$), 8.2 (s, CH$_2$–

Si(OMe)$_3$). ^{31}P{^{1}H} NMR (CDCl$_3$): δ = 29.7 (d, $^1J_{RhP}$ = 126.2 Hz). IR (KBr): $\tilde{v}$ = 1966

(C≡O) cm^{-1}. MS (FAB); m/z: 1042 [M$^+$], 1014 [M$^+$ – CO]. Anal. Calc. (C$_{51}$H$_{62}$ClO$_7$P$_2$RhSi$_2$): C 58.70; H 5.99. Found: C 57.68 [115]; H 5.94.

3.2.1.8. *Carbonylchlorobis[diphenyl[4-[4-(trimethoxysilyl)butyl]phenyl]phosphane-*
κP]iridium(I) [14(T^0)]

In a three-necked flask 350.0 mg (0.390 mmol) of [Ir(COE)$_2$Cl]$_2$ was suspended in 10 mL of acetonitrile. After 10 min argon was replaced by carbon monoxide. Undissolved [Ir(COE)$_2$Cl]$_2$ disappeared immediately, and a yellow solution was obtained, which indicated the formation of [Ir(CO)$_2$Cl]$_2$. After 10 min under an atmosphere of CO 684.3 mg (156 mmol) of the T-silyl functionalized triphenylphoshine **10(T^0)** was added. The color of the solution changed to brown yellow. According to the ^{31}P {^{1}H} NMR and IR spectra the reaction was finished after 20 min. The complex **14(T^0)** was sol-gel processed without further purification. – ^{31}P{^{1}H} NMR (C$_6$D$_6$): δ = 24.7 (s). IR (KBr): $\tilde{v}$ = 1966 (C≡O) cm^{-1}.

3.2.2. Synthesis of the Xerogels

3.2.2.1. *General Procedure for the Sol-Gel Processing of X2a, X2b, X3a, X3b, X3c, and*
X3d

To a solution of **2(T^0)**, **3(T^0)** in 6 ml of THF the corresponding amount of the co-condensation agent **4(D^0)**, **4(T^0)**, **5(D^0)**, and **5(T^0)**, 1.0 g (56 mmol) of H$_2$O and the catalyst tetrabutylammoniumfluoride (TBAF) (0.1 ml of a 1 M solution in THF) was added. The reaction mixture was stirred at room temperature for 24 h until a gel was formed.

Subsequently the solvent was removed under reduced pressure and the crude product was dried for 2 h. After washing three times with methanol (5 ml) and *n*-hexane (5 ml) and drying in vacuum for 4 h the xerogels were obtained as yellow powders.

X2a: Initial weight of **2(T^0)** 101 mg (0.2 mmol) and of **4(D^0)** 145 mg (0.5 mmol). Yield: 153 mg. ^{31}P CP/MAS NMR: $\delta = -6.3$. ^{13}C CP/MAS NMR: $\delta = 156.7$ (NH–CO–NH), 139.0 – 118.5 (br, C–phenyl), 57.8 (O–CH_2–CH_3), 42.3 – 17.8 (br, CH_2 of backbone and spacer), –0.3 (Si–CH_3). ^{29}Si CP/MAS NMR: $\delta = -4.8$ (D^0), -14.3 (D^1), -22.3 (D^2), -58.2 (T^2), -67.7 (T^3).

X2b: Initial weight of **2(T^0)** 101 mg (0.2 mmol) and of **5(D^0)** 184 mg (0.5 mmol). Yield: 162 mg. ^{31}P CP/MAS NMR: $\delta = -6.7$. ^{13}C CP/MAS NMR: $\delta = 156.1$ (NH–CO–NH), 133.0 – 119.0 (br, C–phenyl), 57.7 (O–CH_2–CH_3), 38.9 – 17.8 (br, CH_2 of backbone and spacer), –0.5 (Si–CH_3). ^{29}Si CP/MAS NMR: $\delta = -4.9$ (D^0), -14.4 (D^1), -21.9 (D^2), -57.5 (T^2), -66.8 (T^3).

X3a: Initial weight of **3(T^0)** 73 mg (0.06 mmol) and of **4(D^0)** 353 mg (1.2 mmol). Yield: 321 mg. ^{31}P CP/MAS NMR: $\delta = 29.1$. ^{13}C CP/MAS NMR: $\delta = 156.0$ (NH–CO–NH), 143.8 – 117.6 (br, C–phenyl), 55.2 (O–CH_2–CH_3), 33.3 – 17.6 (br, CH_2 of backbone and spacer), – 0.4 (Si–CH_3). ^{29}Si CP/MAS NMR: $\delta = -12.3$ (D^1), -22.0 (D^2), -59.2 (T^2), -68.6 (T^3). IR (KBr, cm^{-1}): 1982 [ν(Rh–C≡O)].

X3b: Initial weight of **3(T^0)** 75 mg (0.06 mmol) and of **5(D^0)** 457 mg (1.2 mmol). Yield: 355 mg. ^{31}P CP/MAS NMR: $\delta = 28.9$. ^{13}C CP/MAS NMR: $\delta = 156.6$ (NH–CO–NH), 139.5 – 118.2 (br, C–phenyl), 38.8 – 17.1 (br, CH_2 of backbone and spacer), – 0.5 (Si–CH_3).

^{29}Si CP/MAS NMR: $\delta = -4.9$ (D^0), -14.4 (D^1), -21.9 (D^2), -57.5 (T^2), -66.8 (T^3). IR (KBr, cm^{-1}): 1982 [ν(Rh–C≡O)].

X3c: Initial weight of **3(T^0)** 50 mg (0.04 mmol) and of **4(T^0)** 269 mg (0.8 mmol). Yield: 237 mg. ^{31}P CP/MAS NMR: $\delta = 29.6$. ^{13}C CP/MAS NMR: $\delta = 155.1$ (NH–CO–NH), 135.8 – 118.3 (br, C–phenyl), 31.5 – 12.7 (br, CH$_2$ of backbone and spacer). ^{29}Si CP/MAS NMR: $\delta = -56.6$ (T^2), -65.6 (T^3). IR (KBr, cm^{-1}): 1980 [ν(Rh–C≡O)].

X3d: Initial weight of **3(T^0)** 75 mg (0.06 mmol) and of **5(T^0)** 497 mg (1.2 mmol). Yield: 385 mg. ^{31}P CP/MAS NMR: $\delta = 29.0$. ^{13}C CP/MAS NMR: $\delta = 156.1$ (NH–CO–NH), 139.5 – 118.0 (br, C–phenyl), 37.4 – 12.8 (br, CH$_2$ of backbone and spacer). ^{29}Si CP/MAS NMR: $\delta = -56.8$ (T^2), -65.6 (T^3). IR (KBr, cm^{-1}): 1981 [ν(Rh–C≡O)].

3.2.2.2. Synthesis of the Xerogel X4

In a 100 mL Schlenk-tube 5 ml of the crude solution of **14(T^0)** in acetonitrile (441.7 mg, 0.39 mmol) was added to 4 ml of THF. Subsequently 784.9 mg (195 mmol) of the co-condensation agent **5(T^0)** was reacted with the above-mentioned mixture in the presence of 1 ml of water and of 0.1 ml of a 0.1 M solution of tetrabutylammoniumfluoride (TBAF) in THF as the catalyst. Stirring overnight afforded a light yellow gel. Liquid constituents were separated from the crude gel by filtration (P3) and the product was washed three times each with 10 mL of THF and 10 ml of *n*-hexane. Finally the xerogel was dried in vacuum for 4 h and was obtained as a yellow powder. Yield: 895.1 mg. – ^{13}C CP/MAS NMR: $\delta = 139.3$, 128.3 (C-phenyl, backbone and ligand), 37.9, 25.2, 12.9 (CH$_2$, backbone and spacer).

^{29}Si CP/MAS NMR: δ = –56.6 (T^2), – 65.7 (T^3). ^{31}P CP/MAS NMR: δ = 24.4. IR (KBr): 1965 [ν(C≡O)].

3.2.2.3. General Procedure for the Synthesis of the Xerogels X5, X6, X8, and X9 (Gaseous/Solid Interphases)

100.0 mg of **X4** was placed in a 100 ml Schlenk-tube with a magnetic stirring bar. Subsequently argon was replaced by the respective gaseous reactants at room temperature. After removal of excess reactant by argon the xerogels **X5**, **X6**, **X8**, and **X9** were obtained. In the case of the polymers **X5** and **X6** the yields were quantitative.

X5: **X4** was treated with hydrogen chloride. Yield: 101.2 mg. – ^{31}P CP/MAS NMR: δ = –3.2. IR (KBr): 2043 [ν(C≡O)].

X6: **X4** was treated with chlorine. Yield: 102.1 mg. – ^{31}P CP/MAS NMR: δ = –20.4. IR (KBr): 2071 [ν(C≡O)].

X8: **X4** was treated with sulfur dioxide. Yield: 101.6 mg. – ^{31}P CP/MAS NMR: δ = 23.9 (**X4**), 7.8 (**X8**). IR (KBr): 2018 [ν(C≡O)].

X9: **X4** was treated with oxygen. Yield: 101.6 mg. – ^{31}P CP/MAS NMR: δ = 24.1 (**X4**), 3.0 (**X9**). IR (KBr): 2008 [ν(C≡O)].

3.2.2.4. General Procedure for the Synthesis of the Xerogels X7 and X10 and Treatment of X4 with Tetrachloroethane (Liquid/Solid Interphases)

A suspension of 100.0 mg of **X4** in 5 ml of benzene was treated with 0.5 ml of methyl iodide, $^{13}CH_3I$, dicyanoethyne, and tetrachloroethane, respectively, and stirred for 24 h at ambient temperature. The liquid constituents were removed by filtration (P3) and after drying under vacuum the respective xerogels were obtained.

X7: **X4** was reacted with CH_3I and $^{13}CH_3I$, respectively. Yield: 96.4 mg (96.3 mg – $^{13}CH_3I$). – ^{13}C CP/MAS NMR: 139.1 (139.4*), 128.6 (128.3*) (C-phenyl, backbone and ligand), 50.1 (50.1*) (OCH_3), 37.6 (38.2*), 24.5 (24.9*), 12.5 (12.7*) (CH_2, backbone and spacer), –5.1 ($^{13}CH_3$-Ir), * data for the ^{13}C labeled compound. – ^{31}P CP/MAS NMR: δ = –20.2. – IR (KBr): nu(tilde) = 2042 (C≡O) cm^{-1}.

X10: **X4** was reacted with dicyanoethyne. Yield: 95.8 mg. – ^{31}P CP/MAS NMR: δ = –3.3. – IR (KBr): nu(tilde) = 2192 (C≡N), 2014 (C≡O) cm^{-1}.

Behavior of X4 Toward Tetrachloroethane: **X4** was reacted with tetrachloroethane. Yield: 96.7. – ^{31}P CP/MAS NMR: δ = –3.5 (**X5**), –18.3 (**X6**). – IR (KBr): nu(tilde) = 2070, 2043 (C≡O) cm^{-1}.

3.2.2.5. General Procedure for the Sol-Gel Processes of the Stationary Phases X_n11-X_n13 (n = 9, 15, 19)

To a 0.27 M solution of *n*-hexadecylamine in a 55:45 EtOH(95 %)/H_2O mixture the monomeric precursors were added. This mixture was stirred for 24 h at room temperature until a gel was formed. Then the solvent was removed under reduced pressure. For the removal of *n*-hexadecylamine the crude xerogels were placed in a Soxhlet extractor containing 300 ml ethanol and the mixture was refluxed for 3 d. Subsequently the gels were washed three times with *n*-hexane (10 ml) and dried under vacuum for 12 h.

Polysiloxanyloctane(Q^k) (X_911). A mixture of 468.8 mg (2.0 mmol) of *n*-octyltrimethoxysilane and 3.75 g (18.0 mmol) of TEOS in 20 ml of a 0.27 M solution of *n*-hexadecylamine in an ethanol/water mixture was sol-gel processed to yield a colorless swollen gel. After purification and drying 1.95 g of a colorless powder were formed. ^{13}C CP/MAS NMR: δ = 12.2 (SiCH$_2$, CH$_3$), 17.1 (OCH$_2$*C*H$_3$), 22.5 (CH$_2$), 29.4 (CH$_2$), 32.1 (CH$_2$), 59.1 (OCH$_2$). ^{29}Si CP/MAS NMR: δ = –56.4 (T^2), –65.1 (T^3), –93.1 (Q^2), –101.1 (Q^3), –109.9 (Q^4).

Polysiloxanyloctane(Q^k) ($X_{15}11$). A mixture of 468.8 mg (2.0 mmol) of *n*-octyltrimethoxysilane and 6.25 g (30.0 mmol) of TEOS in 32 ml of a 0.27 M solution of *n*-hexadecylamine in an ethanol/water mixture was sol-gel processed to yield a colorless swollen gel. After purification and drying 2.97 g of a colorless powder were formed. ^{13}C CP/MAS NMR: δ = 12.1 (SiCH$_2$, CH$_3$), 16.1 (OCH$_2$*C*H$_3$), 22.3 (CH$_2$), 29.0 (CH$_2$), 31.9 (CH$_2$), 59.1 (OCH$_2$). ^{29}Si CP/MAS NMR: δ = –56.2 (T^2), –64.8 (T^3), –93.5 (Q^2), –101.2 (Q^3), –109.9 (Q^4).

Polysiloxanyloctane(Q^k) ($X_{19}11$). A mixture of 468.8 mg (2.0 mmol) of *n*-octyltrimethoxysilane and 7.91 g (38.0 mmol) of TEOS in 40 ml of a 0.27 M solution of *n*-hexadecylamine in an ethanol/water mixture was sol-gel processed to yield a colorless swollen gel. After purification and drying 3.65 g of a colorless powder were formed. ^{13}C CP/MAS NMR: δ = 12.0 (SiCH$_2$, CH$_3$), 15.6 (OCH$_2$*C*H$_3$), 22.1 (CH$_2$), 28.9 (CH$_2$), 31.8 (CH$_2$), 59.0 (OCH$_2$). ^{29}Si CP/MAS NMR: δ = –56.1 (T^2), –64.8 (T^3), –93.9 (Q^2), –101.3 (Q^3), –110.0 (Q^4).

Polysiloxanyldodecane(Q^k) (X_912). A mixture of 672.1 mg (2.0 mmol) of *n*-dodecyltriethoxysilane and 3.75 g (18.0 mmol) of TEOS in 20 ml of a 0.27 M solution of *n*-hexadecylamine in an ethanol/water mixture was sol-gel processed to yield a colorless swollen gel. After purification and drying 2.07 g of a colorless powder were formed. ^{13}C CP/MAS NMR: δ = 12.3 (SiCH$_2$, CH$_3$), 16.3 (OCH$_2$*C*H$_3$), 22.4 (CH$_2$), 29.5 (CH$_2$), 32.0 (CH$_2$), 59.1 (OCH$_2$). ^{29}Si CP/MAS NMR: δ = –55.7 (T^2), –64.3 (T^3), –92.8 (Q^2), –101.0 (Q^3), –109.8 (Q^4).

Polysiloxanyldodecane(Q^k) ($X_{15}12$). A mixture of 672.1 mg (2.0 mmol) of *n*-dodecyltriethoxysilane and 6.25 g (30.0 mmol) of TEOS in 32 ml of a 0.27 M solution of *n*-hexadecylamine in an ethanol/water mixture was sol-gel processed to yield a colorless swollen gel. After purification and drying 3.14 g of a colorless powder were formed. ^{13}C CP/MAS NMR: δ = 12.3 (SiCH$_2$, CH$_3$), 16.0 (OCH$_2$*C*H$_3$), 22.4 (CH$_2$), 29.5 (CH$_2$), 32.0 (CH$_2$), 59.1 (OCH$_2$). ^{29}Si CP/MAS NMR: δ = –57.8 (T^2), –65.3 (T^3), –93.9 (Q^2), –101.5 (Q^3), –110.0 (Q^4).

Polysiloxanyldodecane(Q^k) ($X_{19}12$). A mixture of 672.1 mg (2.0 mmol) of *n*-dodecyltriethoxysilane and 7.91 g (38.0 mmol) of TEOS in 40 ml ml of a 0.27 M solution of *n*-hexadecylamine in an ethanol/water mixture was sol-gel processed to yield a colorless swollen gel. After purification and drying 3.87 g of a colorless powder were formed. ^{13}C

CP/MAS NMR: δ = 12.2 (SiCH$_2$, CH$_3$), 15.9 (OCH$_2$CH$_3$), 22.3 (CH$_2$), 29.5 (CH$_2$), 32.0 (CH$_2$), 59.1 (OCH$_2$), 64.9 (OCH$_2$). ^{29}Si CP/MAS NMR: δ = –56.7 (T^2), –64.9 (T^3), –93.4 (Q^2), –101.2 (Q^3), –110.1 (Q^4).

Polysiloxanyloctadecane(Q^k) (X$_9$13). A mixture of 833.4 mg (2.0 mmol) of *n*-octadecyltriethoxysilane and 3.75 g (18.0 mmol) of TEOS in 20 ml of a 0.27 M solution of *n*-hexadecylamine in an ethanol/water mixture was sol-gel processed to yield a colorless swollen gel. After purification and drying 2.21 g of a colorless powder were formed. ^{13}C CP/MAS NMR: δ = 12.3 (SiCH$_2$, CH$_3$), 15.9 (OCH$_2$CH$_3$), 22.4 (CH$_2$), 29.8 (CH$_2$), 32.0 (CH$_2$), 59.0 (OCH$_2$). ^{29}Si CP/MAS NMR: δ = –57.6 (T^2), –65.6 (T^3), –93.7 (Q^2), –101.4 (Q^3), –109.9 (Q^4).

Polysiloxanyloctadecane(Q^k) (X$_{15}$13). A mixture of 833.4 mg (2.0 mmol) of *n*-octadecyltriethoxysilane and 6.25 g (30.0 mmol) of TEOS in 32 ml of a 0.27 M solution of *n*-hexadecylamine in an ethanol/water mixture was sol-gel processed to yield a colorless swollen gel. After purification and drying 3.12 g of a colorless powder were formed. ^{13}C CP/MAS NMR: δ = 13.4 (SiCH$_2$, CH$_3$, OCH$_2$CH$_3$), 15.7 (OCH$_2$CH$_3$), 22.4 (CH$_2$), 29.7 (CH$_2$), 32.1 (CH$_2$), 59.1 (OCH$_2$), 65.9 (OCH$_2$). ^{29}Si CP/MAS NMR: δ = –57.6 (T^2), –65.4 (T^3), –93.6 (Q^2), –101.3 (Q^3), –110.1 (Q^4).

Polysiloxanyloctadecane(Q^k) (X$_{19}$13). A mixture of 833.4 mg (2.0 mmol) of *n*-octadecyltriethoxysilane and 7.91 g (38.0 mmol) of TEOS in 40 ml of a 0.27 M solution of *n*-hexadecylamine in an ethanol/water mixture was sol-gel processed to yield a colorless swollen gel. After purification and drying 3.96 g of a colorless powder were formed. ^{13}C CP/MAS NMR: δ = 13.4 (SiCH$_2$, CH$_3$, OCH$_2$CH$_3$), 15.8 (OCH$_2$CH$_3$), 22.3 (CH$_2$), 29.8 CH$_2$), 32.0 (CH$_2$), 59.0 (OCH$_2$), 65.8 (OCH$_2$). ^{29}Si CP/MAS NMR: δ = –57.6 (T^2), –65.6 (T^3), –93.7 (Q^2), –101.5 (Q^3), –110.2 (Q^4).

4. REFERENCES

[1]   P. Panster, S. Wieland, in: *Applied Homogeneous Catalysis with Organometallic Compounds*, Cornils, B.; Herrmann, W. A., Eds.; VCH: Weinheim, Germany, 1996, 605.

[2]   F. R. Hartley, P. N. Vezey, *Adv. Organomet. Chem.* **1977**, *15*, 189.

[3]   J. H. Clark, D. J. Macquarrie, *Chem. Soc. Rev.* **1996**, *96*, 303.

[4]   M. E. Davies, *Chemtech* **1992**, 498.

[5]   W. Dumont, J.–C. Poulin, T.–P. Dang, H. B. Kagan, *J. Am. Chem. Soc.* **1973**, *95*, 8295.

[6]   D. E. Bergbreiter, R. Chandran, *J. Am. Chem. Soc.* **1987**, *109*, 174.

[7]   F. R. Hartley, P. N. Vezey, *Adv. Organomet. Chem.* **1977**, *15*, 189.

[8]   F. R. Hartley, Supported Metal Complexes, D. Reidel Publishing Company, Dordrecht, 1985.

[9]   D. W. Sindorf, G. E. Maciel, *J. Am. Chem. Soc.* **1983**, *105*, 3767.

[10] S. C. Bourque, H. Alper, L. E. Manzer, P. Arya, *J. Am. Chem. Soc.* **2000**, *122*, 956.

[11] J. L. G. Fierro, M. D. Merchan, S. Rojas, P. Terreros, *J. Mol. Catal. A* **2001**, *166*, 255.

[12] P. M. Price, J. H. Clark, D. J. Macquarrie, *J. Chem. Soc., Dalton Trans.* **2000**, 101.

[13] C. Merckle, S. Haubrich, J. Blümel, *J. Organomet. Chem.* **2001**, *627*, 44.

[14] U. Schubert, *New J. Chem.* **1994**, *18*, 1049.

[15] J. Schwarz, V. P. W. Böhm, M. G. Gardiner, M. Grosche, W. A. Herrmann, W. Hieringer, G. Raudaschl–Sieber, *Chem. Eur. J.* **2000**, *6*, 1773.

[16] I. S. Khatib, R. V. Parish, *J. Organomet. Chem.* **1989**, *369*, 9.

[17] E. Lindner, F. Auer, T. Schneller, H. A. Mayer, *Angew. Chem. Int. Ed.* **1999**, *38*, 2154.

[18] U. Deschler, P. Kleinschmitt, P. Panster, *Angew. Chem. Int. Ed.* **1986**, *25*, 237.

[19] E. Lindner, A. Bader, H. A. Mayer, *Z. Anorg. Allg. Chem.* **1991**, *598/599*, 235.

[20] E. Lindner, A. Bader, H. A. Mayer, *Inorg. Chem.* **1991**, *30*, 3783.

[21] E. Lindner, M. Kemmler, H. A. Mayer, P. Wegner, *J. Am. Chem. Soc.* **1994**, *116*, 348.

[22] E. Lindner, A. Jäger, T. Schneller, H. A. Mayer, *Chem. Mater.* **1997**, *9*, 81.

[23] C. J. Brinker, G. W. Scherer, Sol Gel Science; Academic Press: London, 1990.

[24] B. Breitscheidel, J. Zieder, U. Schubert, *Chem. Mater.* **1991**, *3*, 559.

[25] R. J. P. Corriu, C. Hoarau, A. Mehdi, C. Reye, *J. Chem. Soc., Chem. Commun.* **2000**, 71.

[26] J. Büchele, H. A. Mayer, *J. Chem. Soc., Chem. Commun.* **1999**, 2165.

[27] E. Lindner, R. Schreiber, M. Kemmler, T. Schneller, H. A. Mayer, *Chem. Mater.* **1995**, *7*, 951.

[28] E. Lindner, T. Schneller, H. A. Mayer, H. Bertagnolli, T. S. Ertel, W. Hörner, *Chem. Mater.* **1997**, *9*, 1524.

[29] E. Lindner, A. Baumann, P. Wegner, H. A. Mayer, U. Reinöhl, A. Weber, T. S. Ertel, H. Bertagnolli, *J. Mater. Chem.* **2000**, *10*, 1655.

[30] E. Lindner, T. Schneller, F. Auer, P. Wegner, H. A. Mayer, *Chem. Eur. J.* **1997**, *3*, 1833.

[31] E. Lindner, A. Jäger, F. Auer, P. Wegner, H. A. Mayer, A. Benez, D. Adam, E. Plies, *Chem. Mater.* **1998**, *10*, 217.

[32] E. Lindner, F. Auer, A. Baumann, P. Wegner, H. A. Mayer, H. Bertagnolli, U. Reinöhl, T. S. Ertel, A Weber, *J. Mol. Catal. A* **2000**, *157*, 97.

[33] E. Lindner, S. Brugger, S. Steinbrecher, E. Plies, M. Seiler, H. Bertagnolli, P. Wegner, H. A. Mayer, *Inorg. Chim. Acta* **2002**, *327*, 54.

[34] C. A. Fyfe, Solid State NMR for Chemists, CRC Press, Gulph, ON, 1984.

[35] G. Engelhardt, D. Michel, High–Resolution NMR of Silicates and Zeolithes, J. Wiley & Sons, Chichester, New York, Brisbane, Toronto, Singapore, 1987.

[36] K. Schmidt–Rohr, H. W. Spiess, Multidimensional Solid State NMR and Polymers, Academic Press, London, 1994.

[37] D. W. Sindorf, G. E. Maciel, *J. Am. Chem. Soc.* **1983**, *105*, 3767.

[38] E. Bayer, K. Albert, J. Reiners, M. Nieder, D. Müller, *J. Chromatogr.* **1983**, *33*, 197.

[39] R. K. Harris, *Analyst* **1985**, *110*, 649.

[40] E. Lindner, S. Brugger, S. Steinbrecher, E. Plies, H. A. Mayer, *Z. Anorg. Allg. Chem.* **2001**, *627*, 1731.

[41] E. Lindner, W. Wielandt, A. Baumann, H. A. Mayer, U. Reinöhl, A. Weber, T. S. Ertel, H. Bertagnolli, *Chem. Mater.* **1999**, *11*, 1833.

[42] D. Evans, J. A. Osborn, G. Wilkinson, *J. Chem. Soc. A* **1968**, 3133.

[43] M. Beller, B. Cornils, C. D. Frohning, C. W. Kohlpaintner, *J. Mol. Catal. A* **1995**, *104*, 17.

[44] L. A. van der Veen, P. C. J. Kamer, P. W. N. M. van Leeuwen, *Organometallics* **1999**, *18*, 4765.

[45] E. Lindner, T. Salesch, F. Hoehn, H. A. Mayer, *Z. Allg. Anorg. Chem.* **1999**, *625*, 2133.

[46] H.-J. Egelhaaf, E. Holder, P. Herman, H. A. Mayer, D. Oelkrug, E. Lindner, *J. Mater. Chem.* **2001**, *11*, 2445.

[47] E. Lindner, T. Salesch, *J. Organomet. Chem.* **2001**, *628*, 151.

[48] K. G. Allum, R. D. Hancock, I. V. Howell, S. McKenzie, R. C. Pitkethly, P. J. Robinson, *J. Organomet. Chem.* **1975**, *87*, 203.

[49] D. Roberto, E. Cariati, R. Psaro, R. Ugo, *Organometallics* **1994**, *13*, 4227.

[50] K. D. Schramm, T. H. Tulip, J. A. Ibers, *Inorg. Chem.* **1980**, *19*, 3183.

[51] L. Vaska, J. W. DiLuzio, *J. Am. Chem. Soc.* **1961**, *83*, 2784.

[52] M. Rance, R. A. Byrd, *J. Magn. Res.* **1983**, *52*, 221.

[53] M. Mehring, *Principles of High Resolution NMR in Solids,* 2nd ed., Springer–Verlag, Berlin, 1983.

[54] R. Voelkel, *Angew. Chem. Int. Ed.* **1988**, *27*, 1468.

[55] R. S. Aujla, R. K. Harris, K. J. Packer, M. Parameswaran, B. J. Say, A. Bunn, M. E. A. Cudby, *Polym. Bull.* **1982**, *8*, 253.

[56] R. A. Vanderpool, H. B. Abrahamson, *Inorg. Chem.* **1985**, *24*, 2985.

[57] I. M. Al-Najjar, *Inorg. Chim. Acta* **1987**, *127*, L47.

[58] L. Vaska, *Acc. Chem. Res.* **1968**, *1*, 335.

[59] G. L. McClure, W. H. Baddley, *J. Organomet. Chem.* **1971**, *27*, 155.

[60] F. Demartin, N. Masciocchi, *Acta Cryst. C* **1983**, *39*, 1225.

[61] A. M. Mueting, P. Boyle, L. H. Pignolet, *Inorg. Chem.* **1984**, *23*, 44.

[62] C. S. Chin, M. Lee, M. Oh, G. Won, M. Kim, Y. J. Park, *Organometallics* **2000**, *19*, 1572.

[63] W. Stoeber, A. Fink, E. Bohn, *J. Colloid Interface Sci.* **1968**, *26*, 62.

[64] J. S. Beck, J. C. Vartuli, W. J. Roth, M. E. Leonowicz, C. T. Kresge, K. D. Schmitt, C. T.-W. Chu, D. H. Olson, E. W. Sheppard, S. B. McCullen, J. B. Higgins, J. L. Schlenker, *J. Am. Chem. Soc.* **1992**, *114*, 10834.

[65] C. T. Kresge, M. E. Leonowicz, W. J. Roth, J. C. Vartuli, J. S. Beck, *Nature* **1992**, *359*, 710.

[66] A. Monnier, F. Schüth, Q. Huo, D. Kumar, D. Margolese, R. S. Maxwell, G. D. Stucky, *Science* **1993**, *261*, 1299.

[67] S. Inagaki, S. Ogata, Y. Goto, Y. Fukushima, in *Mesoporous Molecular Sieves, Studies in Surface Science and Catalysis*, Vol. 117 (Eds: L. Bonneviot, F. Beland, C. Danumah, S. Giasson, S. Kaliaguine), Elsevier Science, Oxford 1998, p. 65.

[68] P. T. Tanev, T. J. Pinnavaia, *Science* **1995**, *267*, 865.

[69] G. Büchel, M. Grün, K. K. Unger, A. Matsumoto, K. Tsutsumi, *J. Supramol. Sci.* **1998**, *5*, 253.

[70] K. W. Gallis, J. T. Araujo, K. J. Duff, J. G. Moore, C. C. Landry, *Adv. Mater.* **1999**, *11*, 1452.

[71] C. Boissière, M. Kümmel, M. Persin, A. Larbot, E. Prouzet, *Adv. Funct. Mater.* **2001**, *11*, 129.

[72] T^n = T type of silicon atom (three oxygen neighbors), n = number of Si-O-Si bonds; Q^k = Q type of silicon atom (four oxygen neighbors), k = number of Si-O-Si bonds.

[73] M. Pursch, L. C. Sander, H.-J. Egelhaaf, M. Raitza, S. A. Wise, D. Oelkrug, K. Albert, *J. Am. Chem. Soc.* **1999**, *121*, 3203.

[74] L. C. Sander, K. E. Sharpless, N. E. Craft, S. A., Wise, *Anal. Chem.* **1994***, 66*, 1667.

[75] K. Kimata, K. Hosoya, N. Tanaka, T. Araki, D. G. Patterson, *J. Chromatogr.* **1992**, *595*, 77.

[76] R. Brindle, K. Albert, *J. Chromatogr. A* **1997**, *757*, 39.

[77] W. Wielandt, A. Ellwanger, K. Albert, E. Lindner, *J. Chromatogr. A* **1998**, *805*, 71.

[78] A. Ellwanger, R. Brindle, K. Albert, *J. High Resolut. Chromatogr.* **1997**, *20*, 39.

[79] J. Y. Ying, C. P. Mehnert, M. S., Wong, *Angew. Chem. Int. Ed.* **1999**, *38*, 56.

[80] D. A. Loy, K. J. Shea, *Chem. Rev.* **1995**, *95*, 1431.

[81] A. Stein, B. J. Melde, R. C. Schroden, *Adv. Mater.* **2000**, *12*, 1403.

[82] R. J. P. Corriu, *Eur. J. Inorg. Chem.* **2000**, *5*, 1109.

[83] S. L. Burkett, S. D. Sims, S. Mann, *Chem. Commun.* **1996**, 1367.

[84] S. D. Sims, S. L. Burkett, S. Mann, *Mater. Res. Soc. Symp. Proc.* **1996**, *431*, 77.

[85] D. J. Macquarrie, *Chem. Commun.* **1996**, 1961.

[86] Q. Huo, D. I. Margolese, G. D. Stucky, *Chem. Mater.* **1996**, *8*, 1147.

[87] R. P. J. Corriu, A. Mehdi, C. Reyé, *C.R. Acad. Sci. Paris, Sér. IIc*, **1999**, 35.

[88] M. H. Lim, C. F. Blanford, A. Stein, *J. Am. Chem. Soc.* **1997**, *119*, 4090.

[89] K. K. Unger, *Porous Silica, Its Properties and Use as Support in Column Liquid Chromatography*, Vol. 16, Elsevier, Amsterdam **1979**.

[90] P. M. Price, J. H. Clark, D. J. Macquarrie, *J. Chem. Soc., Dalton Trans.* **2000**, 101.

[91] K. Moller, T. Bein, *Stud. Surf. Sci. Catal.* **1998**, *117*, 53.

[92] M. Raitza, J. Wegmann, S. Bachmann, K. Albert, *Angew. Chem. Int. Ed.* **2000**, *39*, 3486.

[93] W. Gao, L. Reven, *Langmuir* **1995**, *11*, 1860.

[94] K. Jinno, T. Ibuki, N. Tanaka, M. Okamoto, J. C. Fetzer, W. R. Biggs, P. R. Griffiths, J. M. Ollinger, *J. Chromatogr.* **1989**, *461*, 209.

[95] W. Gao, L. Dickinson, C. Grozinger, F. G. Morin, L. Reven, *Langmuir* **1996**, *12*, 6429.

[96] M. Pursch, L. C. Sander, K. Albert, *Anal. Chem*. **1996**, *68*, 4107.

[97] K. Albert, T. Lacker, M. Raitza, M. Pursch, H.-J. Egelhaaf, D. Oelkrug, *Angew. Chem. Int. Ed.* **1998**, *37*, 777.

[98] S. Bachmann, C. Hellriegel, J. Wegmann, H. Händel, K. Albert, *Solid State Nucl. Magn. Reson.* **2000***, 17*, 39.

[99] G. Horvath, K. J. Kawazoe, *J. Chem. Eng. Jpn.* **1983**, *16*, 470.

[100] P. T. Tanev, M. Chibwe, T. J. Pinnavaia, *Nature* **1994***, 368*, 321.

[101] A. Brockes, *Z. Phys.* **1957**, *149*, 353.

[102] L. Reimer, *Z. Naturforsch. B* **1961**, *16*, 166.

[103] W. Lippert, *Optik* **1962**, *19*, 143.

[104] D. Dorset, *Structural electron crystallography*, Plenum Press, New York **1995**.

[105] L. Reimer, *Z. Naturforsch. A* **1960**, *15*, 405.

[106] Certificate of Analysis, "SRM 869a Column Selectivity Test Mixture for Liquid Chromatography", Standard Reference Materials Program, National Institute of Standards and Technology, Gaithersburg, MD 20899.

[107] Certificate of Analysis, "SRM 1647c Priority Pollutant Polycyclic Aromatic Hydrocarbons (in Acetonitrile)" Standard Reference Materials Program, National Institute of Standards and Technology, Gaithersburg, MD 20899.

[108] T. S. Ertel, H. Bertagnolli, S. Hückmann, U. Kolb, D. Peter, *Appl. Spectrosc.* **1992**, *46*, 690.

[109] M. Newville, P. Livins, Y. Yakobi, J. J. Rehr, E. A. Stern, *Phys. Rev. B* **1993**, *47*, 4126.

[110] S. J. Gurman, N. Binsted, I. Ross, *J. Phys. C* **1986**, *19*, 1845.

[111] L. Reimer, *Scanning Electron Microscopy*, 2nd ed., Springer-Verlag Berlin, Heidelberg, NewYork, 1998.

[112] V.D. Scott, G. Love, *X-ray spectrometry* **1992**, *21*, 27.

[113] J. Wernisch, *X-ray spectrometry* **1985**, *14*, 109.

[114] C. Poehn, J. Wernisch, W. Hanke *X-ray spectrometry* **1985**, *14*, 120.

[115] Although high temperature and V_2O_5 (catalyst) was used for C, H analyses, the carbon values remained low. This is probably due to incomplete combustion, which may be caused by rhodium; (a) T. E. Nappier, D. W. Meek, R. M. Kirchner, J. A. Ibers, J. Am. Chem. Soc. 95 (1973) 4194; (b) W. O. Siegl, S. J. Lapporte, J. P. Collman, Inorg. Chem. 10 (1971) 2158.

5. Summary

In the last years polymer supported catalysts have evolved into an area of intensive research with the goal to combine the advantages of homogeneous and heterogeneous catalysis. The catalysts become easily separable from the reaction products and they can be reused in several runs, but frequently with an essential loss of activity because of metal leaching. In addition very often the reactive centers are not well defined which causes a decrease of the activities and selectivities. So far these drawbacks prevented a commercial application of heterogenized catalysts. A versatile approach to reduce or even eliminate these detriments is the introduction of the concept of an interphase. Interphases are systems in which a stationary phase (comprised of a polymer, spacer, and reactive centers) and a mobile component (gaseous, liquid, or dissolved reactants) penetrate each other on a molecular scale without forming a homogeneous phase.

Typical stationary phases usually are generated by simultaneous co-condensation of T-silyl functionalized transition metal complexes with various bifunctionalized alkoxysilanes. This procedure affords the possibility to modify materials by controlling the mobility of the entire polymer, the density, and the distance of the reactive centers as well as swelling capabilities.

Referring to these findings in the present thesis the concept of interphases was applied to hydroformylation, which is one of the most important industrial catalytic processes. The catalytic activity strongly depends on the mobility of the stationary phase. To achieve a high mobility of the reactive centers it is important, that the spacer is located in the periphery of the ligand system. To meet this goal a novel T-silyl functionalized triphenylphosphine ligand of the type $Ph_2PC_6H_4NHCONH(CH_2)_3Si(OEt)_3$ was prepared, bearing the spacer unit in the *para*–position of only one phenyl ring. Subsequently the catalytically active T-silyl

functionalized carbonylchloro[bis(phosphine)]rhodium(I) complex $ClRh(CO)[Ph_2PC_6H_4NH–$
$CONH(CH_2)_3Si(OEt)_3]_2$ was synthesized. The ligand as well as the Vaska–analogous
rhodium(I) complex were condensed into matrices built by various D- and T-silyl
bifunctionalized co-condensation agents. Structural investigations of these novel stationary
phases were carried out by multinuclear solid state NMR spectroscopy. To study the mobility
of the matrices and active centers detailed dynamic solid state NMR measurements were
undertaken. The mobility of the rhodium containing xerogels were compared with the
dynamics of the sol-gel processed phosphine prior to the employment of these complexes in
the hydroformylation of 1-hexene. The conversions are in the range of approximatly 70 %
(using the D-silyl bifunctionalized co-condensation agents $Me(MeO)_2Si(CH_2)_6Si(MeO)_2Me$
and $Me(MeO)_2Si(CH_2)_3C_6H_4(CH_2)_3Si(MeO)_2Me$ in dichloromethane as solvent) to 100 %
(using the T-silyl bifunctionalized co-condensation agents $(MeO)_3Si(CH_2)_6Si(MeO)_3$ and
$(MeO)_3Si(CH_2)_3C_6H_4(CH_2)_3Si(MeO)_3$ in dichloromethane or toluene as solvent). The best
selectivities for *n*-heptanale (up to 50 %) were obtained with the T-silyl bifunctionalized co-
condensations agents. Altogether a higher cross-linkage of polymers, which are provided
with T-silyl bifunctionalized copolycondensates, is more advantageous under a pressure of 60
bar. The D-silyl bifunctionalized siloxanes, which are more mobile on the NMR time scale
show a lower activity under these medium pressure conditions. Properties like the swelling
capability and the mobility of the different parts of the polymer become less important. The
accessibility of the reactive centers and thus the catalytic activity increase with the more rigid
polymer backbone of T-silyl bifunctionalized co-condensation agents under the described
conditions.

The synthesis of a sol-gel processable triphenylphosphine ligand without heteroatoms
in the spacer unit was a further objective of the present work. For organometallic reactions in
interphases with substrates that attack the urea unit (e.g. methyliodide) the ligand
$Ph_2PC_6H_4NHCONH(CH_2)_3Si(OEt)_3$ has to be changed into a system without any further

functional groups in the spacer unit. In a further part of this thesis a simple method for the preparation of the modified triphenylphosphine $Ph_2PC_6H_4(CH_2)_4Si(OMe)_3$ is presented which is provided with a T-silyl functionalized hydrocarbon spacer in the *para*-position of only one aryl ring. As an example this phosphine ligand was introduced in the rhodium(I) complex $ClRh(CO)[Ph_2PC_6H_4(CH_2)_4Si(OMe)_3]_2$.

A major intrinsic intricacy that may occur in reactions in interphases are diffusion problems which adversely influence the activity of the catalysts. All reactive centers should be readily accessible for substrates. Excellent model systems for accessibility studies represent iridium complexes which are much more stable compared to corresponding rhodium congeners. Therefore the phosphine ligand $Ph_2PC_6H_4(CH_2)_4Si(OMe)_3$ was coordinated to an iridium(I) complex to carry out organometallic model reactions in interphases. After sol-gel processing of $ClIr(CO)[Ph_2PC_6H_4(CH_2)_4Si(OMe)_3]_2$ the resulting stationary phase was examined towards a series of molecules with different shapes and sizes like oxygen, sulfur dioxide, dicyanoethyne, and different halogenated substrates. The copolycondensation of the T-silyl bifunctionalized hydrocarbon $(MeO)_3Si(CH_2)_3C_6H_4(CH_2)_3Si(MeO)_3$ with the T-silyl functionalized iridium(I) system based on the results of the hydroformylation of 1-hexene with the above-mentioned rhodium(I) xerogels. The resulting products were characterized by ^{31}P CP/MAS NMR, IR, EDX, and EXAFS spectroscopy. It could be demonstrated, that all reactive centers were completely accessible for all substrate molecules and in the case of the reversible reactions also with dioxygen and sulfur dioxide. In addition, the substrate molecules were also able to reversibly leave the polysiloxane matrix without any interference.

In the last part of this work thesis the concept of interphases was transferred to stationary phases applied in high performance liquid chromatography (HPLC). Therefore nanostructured, mesoporous inorganic-organic hybrid xerogels were reproducibly synthesized by a sol-gel procedure. For the introduction of long alkyl chains into inorganic polymers trifunctional *n*-alkyltrialkoxysilanes of the type $CH_3(CH_2)_nSi(OR)_3$ (n = 7, 11, 17 ; R = CH_3,

C_2H_5) were co-condensed with $Si(OEt)_4$ (TEOS). The synthetic pathway involves the employment of *n*-hexadecylamine as template and catalyst. The xerogels obtained by the present procedure consist of uniform spherical particles with a diameter of about 1 µm. The composition of the new materials was determined by ^{13}C and ^{29}Si CP/MAS NMR spectroscopy. Moreover, the degree of organization was investigated by X-ray low angle and electron diffraction. In agreement with ^{13}C CP/MAS NMR spectroscopic measurements the alkyl chains form a crystalline arrangement within the silica polymer. Brunauer-Emmett-Teller (BET) adsorption measurements confirm specific surface areas of up to 1400 m^2/g. These novel mesoporous nanostructured materials have been successfully employed in HPLC for the first time. Different Standard Reference Materials (SRM) containing polycyclic aromatic hydrocarbons have been separated with the xerogels described in the present work.

Lebenslauf

Persönliche Daten:

geboren am	30.09.1967 in Pirna
Eltern	Frank Salesch
	Karin Salesch, geb. Thieme
Familienstand	verheiratet, seit September 1999
Staatsangehörigkeit	deutsch

Schulbildung:

1974-1984	Polytechnische Oberschule in Meerane
1984-1986	Erweiterte Oberschule in Glauchau
	Abschluß: Abitur
1986-1989	Wehrdienst – Nationale Volksarmee – 7. Panzerdivison Torgelow

Studium:

1989-1990	Chemie, Martin-Luther-Universität Halle-Wittenberg
1990-1998	Chemie, Eberhard-Karls-Universität Tübingen
Okt. 1992	Diplomvorexamen
Febr. 1998	mündliche Diplomhauptprüfung
März 1998 – Sept. 1998	Diplomarbeit über das Thema „Neue D- und T-funktionalisierte Polysiloxanmatrizen für Reaktionen in Interphasen" bei Prof. Dr. E. Lindner am Institut für Anorganische Chemie der Universität Tübingen
Okt. 1998 – Jan. 2002	Dissertation bei Prof. Dr. E. Lindner am o. g. Institut – Titel: „Synthesis and Characterization of Novel Functionalized Polysiloxanes and Their Application in Model and Catalytic Reactions, and in Chromatography"

Okt. 1998 – Jan. 2002	Assistent und stellvertr. Praktikumsleiter im Anorganisch-Chemischen Praktikum für Fortgeschrittene, Abschnitt Molekülchemie
Okt. 1998 – Jan. 2002	Kollegiat im Graduiertenkolleg „Chemie in Interphasen"
Mai 2000 - Juli 2000	Forschungsaufenthalt an der Universität Montpellier II (Frankreich) bei Prof. Dr. R. J. P. Corriu